Physics – Uspekhi **47** (3) 273 – 288 (2004)

REVIEWS OF TOPICAL PROBLEMS

PACS numbers: **73.50. – h**, 74.25.Op, **74.72. – h**, **74.80. – g**

Dynamic dissipative mixed states in inhomogeneous type II superconductors

V F Khirnyĭ, A A Kozlovskiĭ

DOI: 10.1070/PU2004v047n03ABEH001724

Contents

Abstract. Dynamic dissipative mixed states, energy dissipation, and the penetration of a transport current's self-magnetic field are considered for the following type II superconductors: low temperature small-crystallite metal films, high temperature polycrystalline films, and bulk inhomogeneous (granular) samples. The special transport properties of such superconductors are primarily due to their morphology.

1. Introduction

The dynamic dissipative mixed (DDM) state has been studied rather thoroughly in type I low temperature superconductors (LTSCs) [1] and in transport-current-carrying 'hard' and composite type II LTSCs [2]. Meanwhile, however, many new and interesting results have been obtained in both inhomogeneous (granular) type II LTSCs and in samples of ceramic high temperature superconductors (HTSCs). It is these circumstances, along with the interest in achieving large critical currents in such superconductors, which justify writing this review.

The review examines the transport-current-induced transition from the superconducting (SC) to the DDM state in metallic granular (fine-grained) LTSC films and in layered LTSC and HTSC films (Section 2), as well as in bulk ceramic HTSC samples (Section 3).

V F Khirnyĭ, A A Kozlovskiĭ Institute for Single Crystals, the National Academy of Sciences of Ukraine
Prosp. Lenina 60, 61001 Khar'kov, Ukraine,
Tel. (380-572) 30-83 11
Fax (380-572) 32-02 73
E-mail: khirnyi@isc.kharkov.com

Received 8 August 2003
Uspekhi Fizicheskikh Nauk **174** (3) 285 – 301 (2004)
Translated by E G Strel'chenko; edited by M V Magnitskaya

2. Current field penetration and the DDM state in wide polycrystalline and layered films

2.1 Metastable current states

Before the discovery of HTSCs [3], the properties of DDM states in granular superconductors were mainly studied in fine-grained metal films, with the oxide of the superconductor's material surrounding film crystallites [4]. There are three reasons for the interest in such samples. First, granular films were widely used in fabricating low-temperature devices (kryotrons, etc.). Second, films with the properties of type I and II superconductors could be easily obtained from a bulk type I superconductor by thermal sputtering in a medium or low vacuum [5]. And third, owing to the characteristically low critical currents of the samples, the effects of the pinning forces F_p and of heat release Q on the motion of vortices were reduced to a minimum.

A study of the dissipative state on wide ($w > \xi > \lambda_\perp$) small-crystallite films of Al, In, and Sn in the thickness range $d = 10-300$ nm revealed metastable current states (MSCSs) [5 – 11]. Here, w is the thickness of the film, ξ is the coherence length, $\lambda_\perp = 2\lambda_L^2/d$ is the effective penetration depth for a magnetic field perpendicular to the film, and λ_L is the London penetration depth of a magnetic field. MSCSs on current-voltage ($I-V$) curves were identified as straight lines with different values of dV/dI, where V is the electrical voltage across the sample and I the electrical (transport) current (Fig. 1). The way the MSCSs and voltage steps ΔV appeared on an $I-V$ curve is as follows. As I was increasing toward I_1, the graph of the $I(V)$ dependence was a nearly straight line coinciding with the axis of current. At a voltage V_1, when $I = I_1$, a jump from this near-vertical to the straight line *1* was made by the plotting device's current point. Along the straight line *1*, both motions upward, to the point with the coordinates I_2, V_2, and downward, to $\bar{I}_2$, $\bar{V}_2$, were possible as

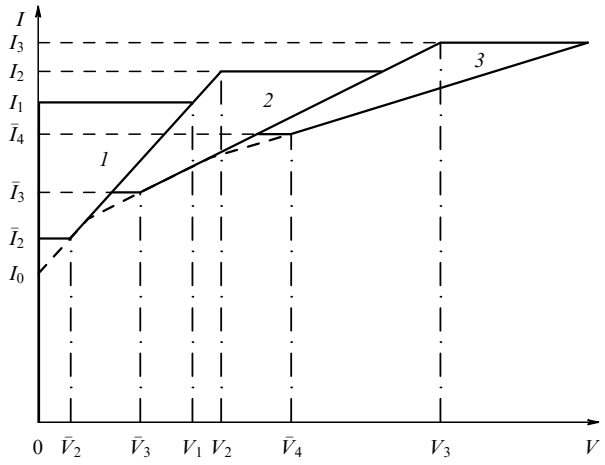

Figure 1. A typical $I-V$ curve for thin-film LTSC samples.

the current was further increased or decreased, respectively. At point I_2, V_2, a jump to the next straight line *2* occurred, and at point $\bar{I}_2$, $\bar{V}_2$, a jump to the preceding (non-dissipative) portion of the $I-V$ curve took place. In a similar way, motions along the straight lines *2* and *3* involved the current point's jumps to the neighboring MSCSs, thus producing a series of such straight (or near-straight) lines.

For films with several potential leads along their length, the SC state was found to be destroyed in transversely arranged narrow strips [6]. This fact was confirmed by tunneling measurements [7]. The local nature of SC suppression was explained [8] as being due to Abrikosov (or A) vortices moving one after another in chains under the action of the transport current (the Lorentz force) and penetrating into the film in its 'current-weak' regions. The uncorrelated appearance of A-vortices at the opposite edges of the film and by pairs is also a possibility [5].

To penetrate the film, A-vortices must overcome an edge barrier [12] of a similar nature to the Bean – Livingston barrier [13], which can be lowered by an inhomogeneity, a magnetic field, or a transport current.

There exist two critical values of the current: I_{c1}, the lower one, at which the barrier sharply decreases but does not disappear completely [14], and I_{c2}, the upper one, at which the barrier decreases to zero [8], enabling the first A-vortex to penetrate the film. The value of I_{c2} was found by minimizing the total derivative of the vortex energy [8],

$$E(x) = \frac{(\Phi_0/4\pi)^2}{\lambda_\perp}\left[\ln\left(\frac{2\lambda_\perp}{\xi}\right) + \frac{\pi}{2}N_0\left(\frac{x}{2\lambda_\perp}\right) + \frac{\pi}{2}E_0\left(\frac{x}{2\lambda_\perp}\right)\right] - \frac{2\Phi_0 I}{\pi c}\left(\frac{x}{w}\right)^{0.5}, \quad (1)$$

for a film with a current in the region $\lambda_\perp \ll x \ll w$ along the x coordinate, where $\Phi_0 = hc/2e$ is the magnetic flux quantum, h is Planck's constant, c is the speed of light in a vacuum, e is the electron charge, and $N_0(z)$ and $E_0(z)$ are the Neumann and Weber functions, respectively [15]. For wide films, with the current flowing primarily along the edges [16], I_{c2} is expressed as [8]

$$I_{c2} = \frac{c\Phi_0}{8\sqrt{2}\,\pi^{0.5}\xi}\,\frac{w}{\lambda_\perp} \sim 1 - \frac{T}{T_c}, \quad (2)$$

where T is the temperature and T_c the critical temperature. This expression agrees with the experimentally obtained dependence

$$I_1(T) = I_c(T) \sim \left(1 - \frac{T}{T_c}\right)$$

up to $T/T_c = 0.7$ (I_c being the critical current). Formula (2) agrees to within a factor ≈ 1 with the estimated value for a film with inhomogeneities [17, 18] of a current at which a current equal to the depairing value I_c^{GL} [19] is achieved at the edges.

In real films, inhomogeneities lower the barrier, and the condition $I_{c1} < I_c < I_{c2}$ is always fulfilled [8]. From formula (1), the deviation of I_{c2} from I was determined [8] in the form $k = a\varkappa(r_D/d)^{0.5}$, where $a \approx 1$, $\varkappa = \lambda_L/\xi$ is the Ginzburg – Landau parameter and r_D the effective size of inhomogeneities in the sample. The straight line in Fig. 2 is the dependence

$$\ln\left[k\left(\frac{d}{d_0}\right)^{0.5}\right] = \ln\left[a\left(\frac{r_D}{d_0}\right)^{0.5}\right] + \ln\varkappa,$$

obtained in Ref. [8] for $r_D = 1.81 \times 10^{-6}$ m, where d_0 is a constant. A similar inhomogeneity size was obtained by a different method in Ref. [20].

As A-vortices move along the film, it has been shown [21] that they interact with one another through empty space. Therefore to increase their linear density it is necessary to apply to the film a voltage $V = \Phi_0/\tau_L(I)$ [22, 23], where $\tau_L(I)$ is the time it takes an A-vortex to travel the intra-chain separation distance. As long as $\tau_L > \tau_0$, the $I-V$ curve is reversible, and the energy released during the motion of A-vortices [8] goes to the thermostat. Here τ_0 is the relaxation time of temperature T to the equilibrium value T_0. For $\tau_L \leqslant \tau_0$, the local temperature T_m along the trajectory of the A-vortices does not have enough time to relax to T_0, leading to a temperature instability there. In this region, a nonuniform longitudinal electric field E develops, and a strip of normal phase appears in the form of a thermal resistive domain. The field penetrates to a depth $l_E = (l_i l_H T/3\varepsilon)^{0.5}$, and it is there that the dissipation of energy takes place [24]. Here l_i is the effective elastic mean free path, l_H is the effective inelastic relaxation length, and ε the energy gap in the elementary excitation spectrum of the superconductor. In the films studies, l_E values ranged from 10^{-6} to 10^{-7} m [9].

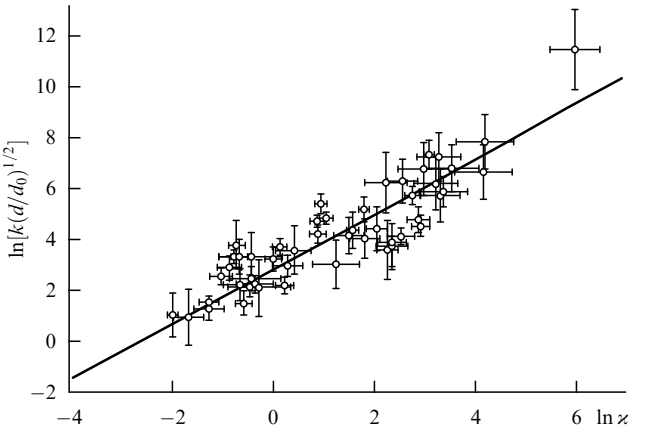

Figure 2. The deviation of the theoretical from the experimental value of critical current as a function of the Ginzburg-Landau parameter.

2.2 Determination of local temperature in the region of suppressed superconductivity

In Ref. [8], T_m was calculated using the heat conduction equation for a one-dimensional (across the film) heat source,

$$\frac{d}{dx}\left[K(T)\,\frac{dT}{dx}\right] - A(T)(T - T_0) + B'\delta(x) = \rho' C\,\frac{\partial T}{\partial t}\,, \quad (3)$$

where $K(T)$ is the film thermal conductivity per unit thickness, x is the coordinate along the length of the film with the heat source at $x = 0$ (Fig. 3), $A(T) = \left[a_1(T) + a_2(T)\right]/d$ is the total coefficient of heat transfer to the substrate (a_1) and the surrounding medium (a_2) per unit thickness, $B' = P/wd$ (P being the power expended by the outer heat source), ρ' is the density of the sample material, C is the heat capacity, and $\delta(x)$ is the delta function. In the films studied, the time of the uniform relaxation of temperature $\tau_0 = \rho' C/A$ as defined from Eqn (3) was $\sim 10^{-9}$ s [9]. Close to T_c, temperature fluctuations are small, $\Delta T_m = (T_m - T_0)$ and K, A are constants, and Eqn (3) becomes [9]

$$K(T_0)\,\frac{d^2(\Delta T)}{dx^2} - A\Delta T = 0 \quad (4)$$

with the boundary conditions

$$\left.\frac{2\,d(\Delta T)}{dx}\right|_{x=0} = \frac{B'}{K}\,, \quad \text{and} \quad \lim_{x \Rightarrow \infty} \Delta T(x) = 0\,, \quad (5)$$

where $T_m = T(x = 0)$. According to Eqn (4), as we move in the direction of x from the heat source located at $x = 0$, the temperature decreases according to the law

$$\Delta T = \Delta T_m \exp\left(-\frac{x}{\lambda_T}\right),$$

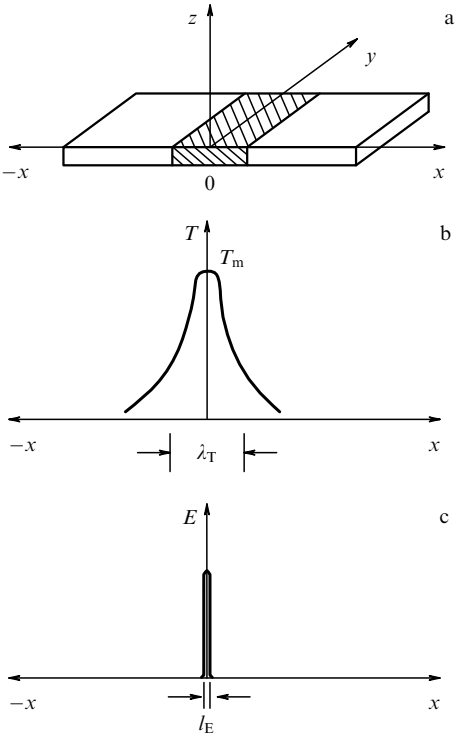

Figure 3. Schematic of (a) the local suppression of superconductivity (dashed region), (b) T_m, local heating temperature, and (c) electric field E.

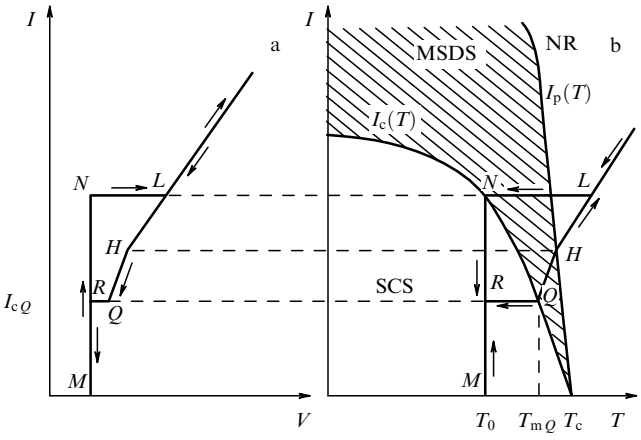

Figure 4. Determining T_m from (a) the $I-V$ curves and (b) the $I-T$ diagram of the samples. SCS: SC state, MSDS: metastable dissipative state, NR: normal region, $I_p(T) = I_c^{GL}(T)$ is the depairing current.

where the heat propagation length $\lambda_T = (K/A)^{0.5}$ of the films studied was $\sim 10^{-5}$ m. The estimates above suggest that $\lambda_T > l_E$, thus validating the δ-function representation of the heat source in Fig. 3 and Eqn (3).

In practice, the films were studied over a wide range of temperatures, and Eqn (4) was replaced by a more general one in which the temperature dependences $K(T)$ and $A(T)$ were included. It therefore proved possible to obtain [8] an expression for finding the value of T_m explicitly:

$$P = R_0\left[3(T_m - T_0)^4 + 8(T_m - T_0)^3(T_0 + \beta) + 6(T_m - T_0)^2(T_0 + \beta)^2\right]^{0.5}. \quad (6)$$

Here $\beta = -0.5T_c$ and the constant R_0 was determined from the $I-V$ curve and the $I-T$ diagram (Fig. 4). Arrows on the $I-V$ curve indicate the variation of I, and those on the $I-T$ diagram show the corresponding change in the local temperature in the region of suppressed superconductivity.

When $I = 0$, the temperature of the film is T_0, to which there corresponds point M in the $I-T$ diagram. For $I = I_N$ there appears a region where the SC state is suppressed, and T_m in a time $\sim \tau_0$ (straight line NL in the $I-V$ curve) generally reaches larger values than T_c (point L at the $I-T$ diagram). As the current further increases, T_m increases monotonically. As the current subsequently decreases, the SC state at point L cannot be restored because we have $T_m > T_c$ there. The equality $T_m = T_c$ is achieved at point H, but the sample does not make a transition to the SC state because $V \neq 0$. This transition occurs only at point Q, when the local temperature T_m relaxes in time $\sim \tau_0$ to the thermostat temperature T_m (straight line QR in the $I-T$ diagram and the $I-V$ curve). The coefficient R_0, as determined from Eqn (6) for $T_0 = 0.5T_c$, is $R_0 = (P_Q/\sqrt{3})(T_{mQ} - T_0)^{-2}$ [8], where P_Q is the power dissipated in the film as calculated for point Q in the $I-V$ curve, and T_{mQ} is the local temperature of the region of suppressed superconductivity, when the current point of the graph plotter recording the $I-V$ curve is at point Q. Knowing R_0, it is possible to determine the value of T_m for any point of the $I-V$ curve between points H and Q. Referring to the T_m dependence for the indium film in Fig. 5, it is seen that λ_T and T_m increase as I increases.

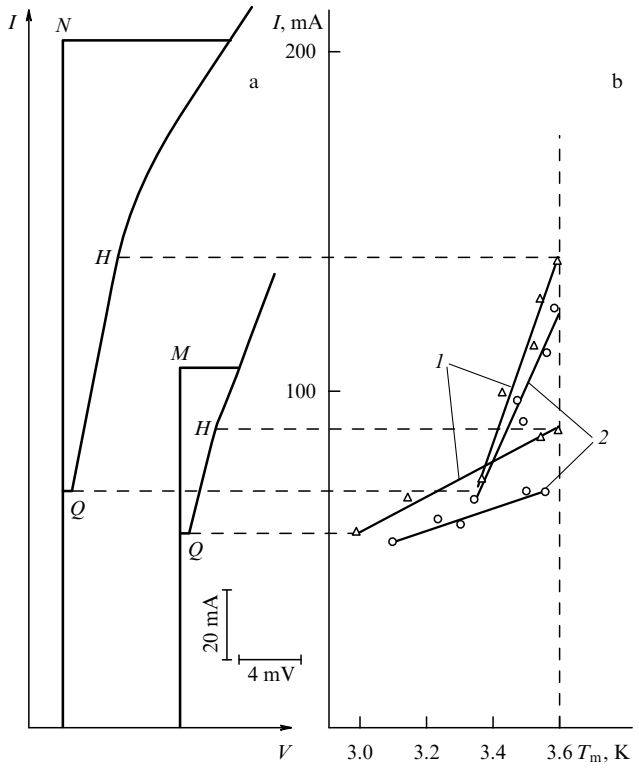

Figure 5. (b) $T_m(I)$ dependence constructed using the $I-V$ curve for an indium film shown in (a). Straight lines *1* are obtained for $T_0 = 2.6$ K; straight lines *2*, for $T_0 = 2$ K.

2.3 $I-V$ curve formation in granular LTSC films

Given the analytical dependences $T(x)$ and $E(x, T, j)$, the $I-V$ curve of a film,

$$V = \int E(x, T, j)\,\mathrm{d}x = \int E(x, T, j)\left(\frac{\mathrm{d}x}{\mathrm{d}T}\right)\mathrm{d}T\,,$$

can be represented by the formula [25]

$$V = 2\int_{T_0}^{T_c(I)} E(T, j)(B')^{0.5}\,K(T)\,\mathrm{d}T + \Delta V_H\,, \qquad (7)$$

where the first term on the right is due to the normal phase strip, and the second arises from the voltage drop across an inhomogeneity.

In the absence of vortex pinning the expression for $E(T, j)$ is written in the form $E = \rho_n f(j, T)$ [26], where ρ_n is the normal state resistivity of the film, j is the average transport current density, and

$$f(j, T) = \frac{(1 - j/j_c)}{[1 - j/j_c + F(j, T)]}\,,$$

where

$$F(j,\ T) = a\left(\frac{j}{j_c}\right)\left[\frac{T_c - T}{T_c}\right]^{3/2}, \qquad a \approx 1\,,$$

j_c is the average critical current density for the DDM state. The nonlinearity of the function $E(j, T)$ is due to the heat production process being nonlinear because of the dissipative effects of the viscous motion of the A-vortices [26, 27].

In Ref. [28] a nonlinear heat production model was employed to obtain the state diagram of a wide LTSC film carrying a transport current. It is shown that at different values of current, the superconducting, resistive, normal, and bistable states are realized in the film. In the latter of these, inhomogeneous switching-wave states exist which translate the film either into the superconducting state (at a certain temperature T_1) or into the resistive or the normal state, depending on the conditions.

What an experimentally obtained $I-V$ curve looks like also depends on the measurement regime used [26, 29]. Thus far, $I-V$ curves obtained in the specified-current regime have been considered. Figure 6 compares two first MSCSs and a portion of the $I-V$ curve measured using a source with, respectively, either the current (curve *1*) or voltage (curve *2*) being specified. When the $I-V$ curve is measured in the specified current regime, the condition $\tau_L < \tau_0$ is fulfilled before the onset of a temperature instability. The frames of the A-vortices are spaced at least about ξ apart. The time electrons stay bound in this region is $\tau_\Delta \approx \hbar/2\varepsilon(T) \approx 10^{-11}$ s [30], where $\hbar$ is Planck's constant. Hence, an A-vortex undergoing isothermal motion must travel a distance ξ in the time the electrons remain bound — giving the maximum velocity $\xi/\tau_\Delta \approx 10^4$ m s^{-1}. On the other hand, when $\tau_L(I) = \tau_0$, the minimum separation between the vortices will be $\approx \lambda_T$, so that the minimum velocity for the non-isothermal motion of the vortices at the moment of formation of a normal phase strip will be $\lambda_T/\tau_0 \approx 10^4$ m s^{-1}, identical to the velocity of isothermal motion as determined by a different method in the discussion above.

At $\tau_L(I) < \tau_0$ (voltage breakdown region between points C and D on curve *1*, see Fig. 6) a strip of normal phase appears. Then the amount of heat that goes to the thermostat from an inhomogeneity exceeds that extracted from a pure superconductor, and the normal phase strip attaches itself to the inhomogeneity and does not expand [31], which is possible if heat propagates diffusively along the film from the heated region [5, 32]. If the current is increased (above point D on

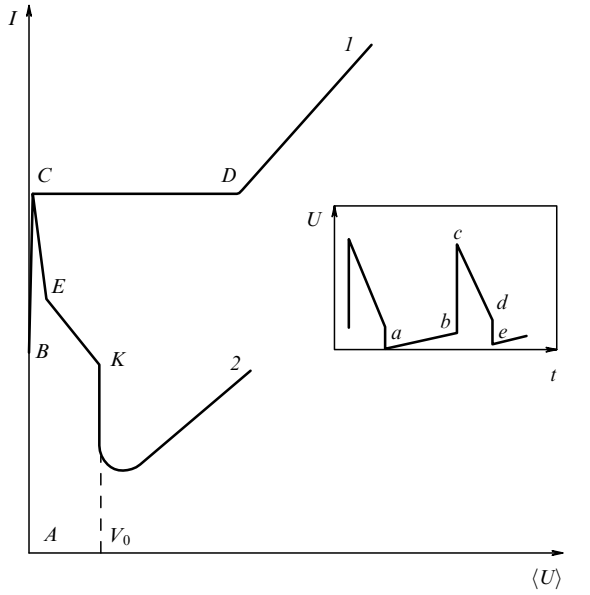

Figure 6. Schematic of the $I-V$ curves measured at a specified current (*1*) and specified voltage (*2*). In the inset the voltage pulse oscillogram of the 'giant Josephson generation' of electromagnetic vibrations is shown.

curve *1*, see Fig. 6), the $I-V$ curve is seen to behave nearly linearly. The linear dependence $I(V)$ means [8] that almost all energy from the emf source is expended to break Cooper pairs in the region where a non-uniform longitudinal electric field exists (see Section 2.1), and that only a fraction of it goes to heating the sample. In this case, when electrons bound in a pair are accelerated by this field over a distance l, they gain energy δW equal to eEl. If $\delta W > 2\varepsilon$ (pair-binding energy), then an individual electron that encounters a defect is scattered, breaking up the pair. Because $eEl = eV$, the minimum voltage V_0 at which there exists a DDM state is given, for decreasing current I, by the expression [8]

$$V_0 = \frac{2\varepsilon(T)}{e}\,. \tag{8}$$

When the $I-V$ curve is measured by specifying the voltage [26, 29], A-vortices penetrate the film when $I = I_B$ (point B on the $I-V$ curve, see Fig. 6) [33]. When $I = I_C$ (point C in Fig. 6) a normal phase strip forms first, causing current I to decrease due to the appearance of an electrical resistance R_n (portion CE of curve *2*, see Fig. 6). Energy dissipation decreases, and the strip returns to the SC state in a time $\sim \tau_0$. At $I = I_B$, the A-vortices will again start penetrating and moving at the same spot on the film (point E in Fig. 6). The oscillogram in the inset of Fig. 6 shows the instantaneous values which the electrical voltage U on the film takes on as A-vortices penetrate the film and move in it forming normal phase strips in doing so [29, 33]. Point a is one where the A-vortices start penetrating, and at point b a temperature instability develops and a strip appears.

At point b the voltage U grows to the value $U = V_0 + U_n + U_p$, where U is the instantaneous value of the voltage drop across the normal phase strip (the magnitude of the pulse front edge), and U_p is the instantaneous voltage drop characterizing the nonequilibrium electric field directed along the flow of the current I from the normal phase strip to the superconducting region. The existence of such a field, l_E away from the normal strip, was assumed earlier in Ref. [24]. Here, it is obtained in a natural way because electrons in the transport current have an energy higher than ε. U_n is the voltage across the strip.

Upon the formation of a normal phase strip (point c in the inset of Fig. 6) the current I will become smaller than I_c, and T_m will become equal to T_0 in a time $\approx \tau_0$. The shape of the dependences $U(t)$ and $R(t)$, however, will be determined by the time it takes the quasiparticles to recombine into pairs by emitting phonons (portion cd in the inset of Fig. 6). In this time $U(t)$ will become equal to V_0 [29] (portion de in the inset of Fig. 6). Because $I < I_c$, superconductivity will restore itself, and $R(t)$ and $U(t)$ will reach the zero value in a time of order τ_Δ (point e in the inset of Fig. 6). At $I = I_B$ the strip formation process will start again and repeat itself periodically, and electromagnetic vibrations will start to be generated on the film [29]. These non-stationary strips have come to be known as 'phase slip strips' (PSSs) [33].

Based on the form of the $I-V$ curve [29], the period t_p for the appearance of a PSS can be obtained from the relation [33]

$$\langle U\rangle = \frac{Ut_i}{t_p} = Ut_i\nu\,,$$

which determines the average voltage $\langle U\rangle$ produced by a pulse generator whose pulses have a duration t_i and an instantaneous voltage amplitude U. Here, ν is the pulse repetition frequency. According to this relation, $\langle U\rangle \sim \nu$; the minimum oscillation frequency is $\nu_{min} \sim 1/w$ because the larger w the larger t_p; ν_{max} is reached when the voltage drop across the superconductor takes the minimum value $\langle U\rangle = V_0$ (point K on the $I-V$ curve, see Fig. 6), above which the transition to the normal state takes place [29, 33].

The way the emergence rate of PSSs is related to magnetic flux Φ piercing them can be found [29] from the Josephson relation $\langle U\rangle = \Phi\nu/c$, where c is the speed of light in a vacuum.

2.4 Features of the SP to DDM state transition in gapless superconductors

The discussion so far has been concerned with superconductors with $\varepsilon \neq 0$. Note, however, that ε depends on T, I, and the magnetic field H. In granular films close to T_c there is a region in the (T, H) plane in which $\varepsilon = 0$, $\Delta \neq 0$, and $l_i < \xi$ [34], where Δ is the order parameter. In this region, according to the 'first equivalence theorem' [35], the electrical conductivity σ of a film is equivalent to that of a superconductor with added paramagnetic impurities, i.e., the state of the film is one of gapless superconductivity [36]. In this state the screening current I_s induced by the field H satisfies the condition $I_s > I_c$ [34], and therefore $I_g > I_c$, where I_g is the generation current of electromagnetic oscillations.

The dependences $I(T)$ and $I(H)$ can be obtained by including the effect of paramagnetic impurities on the thermodynamic properties of a superconductor [34, 37]. Upon adding impurities the expression for the energy gap takes the form [37]

$$\varepsilon_p = \Delta\left[1 - \left(\frac{1}{\tau_s\Delta}\right)^{2/3}\right]^{3/2}, \tag{9}$$

where τ_s is the spin flip mean free path of an electron.

When $\tau_s\Delta = 1$, $\varepsilon_p = 0$ for $\Delta \neq 0$, and the superconductor becomes gapless, but the phenomenon of superfluidity ($R = 0$) persists owing to superconducting correlations between Cooper pairs. The current density in this case can be written in the form [37]

$$\mathbf{J} = \mathbf{J}_s + \mathbf{J}_n\,,$$

where $\mathbf{J}_s = (2\sigma\tau_s/c)|\Delta|^2\mathbf{P}'$, $\mathbf{J}_n = \sigma\mathbf{E}$, $\mathbf{P}' = 2m\mathbf{v}_s$ is the superfluid momentum, and $\mathbf{v}_s$ is the velocity of the superconducting electrons. Close to T_c

$$v_s \sim \frac{\hbar}{m\xi(T)} \sim \Delta(T)\,,$$

$\Delta(T) \sim (1 - T/T_c)^{0.5}$ [34], and $\Delta(H) \sim [1 - (H/H_c)^2]^{0.5}$ [38], where H_c is the thermodynamic critical magnetic field. Hence,

$$J_g(T) \sim \left[\Delta(T)\right]^2 \sim 1 - \frac{T}{T_c}\,, \quad J_g(H) \sim 1 - \left(\frac{H}{H_c}\right)^2, \tag{10}$$

whereas $J_c^{GL}(T) \sim (1 - T/T_c)^{3/2}$, and $J_c^{GL}(H) \sim [1 - (H/H_c)^2]^{3/2}$. Properties like this have been observed in generation current in Ref. [39].

2.5 Features of the SC to DDM state transition close to T_c

The discussion thus far has been concerned with the temperature region $T < 0.9T_c$, for which $\xi(T)$, $\lambda_\perp(T) < r_D$. For $T > 0.9T_c$ and $\xi(T)$, $\lambda_\perp(T) > r_D$, the transverse size of the A-vortices exceeds the size of the inhomogeneities. The

situation in this case is reminiscent of the behavior of A-vortices in a homogeneous film because the vortices do not 'see' inhomogeneities. In such films the barrier to A-vortex penetration decreases by practically the same amount along the whole of the sample due to the transport current only. A-vortices penetrate over the entire length of the film within a small range of critical currents.

When the $I-V$ curve is measured in the fixed-current regime, no A-vortices are present after a temperature instability has developed. The whole of the sample makes a transition to the dissipative state with no motion of magnetic flux and only with a set of normal phase strips, at a distance l_E apart (see Section 2.2). The fact that neither A-vortices nor the magnetic flux move was reported in Ref. [40]. Close to T_c, the separation l_E between the normal phase strips becomes the same order as λ_T due to the increase of l_E ($l_E \sim \varepsilon^{-0.5}$, and $\varepsilon \to 0$ as $T \to T_c$). Hence, we obtain $2l_E$ for the total length of the inhomogeneous state over which there exist an electrical resistance R_r and an electrical voltage V_r. Because the inhomogeneous regions are identical, it is found that the electrical resistance of the film is a multiple of R_r and its $I-V$ is stepwise with a voltage step V_r.

The reader is referred to Ref. [41] for experimental data concerning 1) the existence of an inhomogeneous region of length $2l_E$ with a voltage drop in multiples of V_r on the $I-V$ curve, 2) the increase, in multiples of R_r, of electrical resistance along the film, and 3) the appearance of a stepwise $I-V$ curve close to T_c.

What is characteristic of the $I-V$ curve in this case is the finite value of the superconducting current I_0 (see Fig. 1) as obtained by extrapolating the slope dV/dI to $V = 0$. This phenomenon, however, confirms the existence of normal phase strips because the appearance of the current I_0 is due to the Andreev reflection effect. Electrons are reflected as holes when electrical current flows from the normal to the superconducting region, and, as a result, there are two parts to the supercurrent, the current of Cooper pairs, which is equal to $I_c - I_0$, and the current of holes, I_0. That the values of I_0 are about the same for the first three or five MSCSs is due to the fact that only those electrons with energies less than $\varepsilon(T)$ are reflected.

There is an interesting feature which should be observed when the $I-V$ curve is measured in the fixed voltage regime: for $I < I_c$ (point C in Fig. 6) it is expected that electromagnetic oscillations will start to be generated throughout the sample.

2.6 DDM states in layered superconductors

In layered LTSCs at $T > T_{KT}$, the Berezinskiĭ–Kosterlitz–Thouless transition temperature [42, 43], a quasi-two-dimensional state shows up in a system of neutral pairs of two-dimensional (2D) vortices and antivortices [44–46]. In such materials the current I caused by the breakup of vortex dipoles and by the motion of free two-dimensional A-vortices (whose number depends on the value of I) gives rise to energy dissipation and a nonlinear $I-V$ curve, altering the nature of heat production processes as a consequence. The dependence of V on I has the form [47, 48]

$$V \sim I^{a(T)+1}, \qquad a(T) = \Lambda\left(\frac{T_c - T}{T}\right),$$

$$\Lambda = \Phi_0 \frac{s}{16\pi^2 \lambda_L(0)^2 T_c},$$

where s is the period of the layered structure and $\lambda_L(0)$ is the London penetration depth at 0 K [49].

Besides the above, the interlayer Josephson coupling [50] should be taken into account in considering the thermal stability of the DDM state in layered HTSC samples. In high-temperature superconductors 2D vortices that arise due to thermal fluctuations are closed with two Josephson vortices (D-vortices) located between superconducting layers. For the current I to break such a device it has to overcome the stress of D-vortices. This gives rise to the critical current component $I_c(T) = I_{c0}(1 - T/T_{KT})^{3/2}$ [50], which vanishes for $T = T_{KT}$, and the $I-V$ curve of HTSC samples can be written in the form $V \propto I[I - I_c]^{a(T)}$ [51].

In Ref. [52] the nonlinear nature of heat production is taken into account as follows. Heat production power is written in the form

$$\frac{\partial Q(T)}{\partial t} = \rho(J, T)\, J^2,$$

and the nonlinear resistivity of the superconductor in the dissipative state is taken to be

$$\rho(J, T) = \rho_n \left[1 - \frac{J_c(T)}{J}\right]^{a(T)},$$

with

$$J_c(T) = J_{c0}\left(1 - \frac{T}{T_c}\right).$$

This model, however, ignores the fact that for T_{KT} the current $I_c \to 0$ and that the $I-V$ curve remains nonlinear [53] all the way to $T = T_c > T_{KT}$. Another point to be considered here is the presence of the depairing current I_c^{GL}, which tends to zero at $T = T_c$. And it is only when $I = I_c^{GL}$ that an HTSC makes the transition to the normal state and the $I-V$ curve becomes linear. These features were taken into account in Refs [54, 55]. The former was concerned with the solution of a one-dimensional equation of the type (3) which employed an expression for the effective nonlinear electrical resistivity of a superconductor $\rho(J, T)$ to approximate the main features of the behavior of layered HTSCs. In Ref. [55], resistivity in the resistive state was taken to be

$$\rho(J, T) = \rho_n \frac{J - J_c(T)}{[J_c^{GL}(T) - J_c(T)]^{a(J,T)}},$$

where

$$a(J, T) = \left(\frac{T_c - T}{T}\right)\left\{1 - \left[\frac{J}{J_c^{GL}(T)}\right] b\right\},$$

b is a numerical parameter,

$$J_c^{GL}(T) = J_c^{GL}(0)\left(1 - \frac{T}{T_c}\right)^{3/2}$$

and $J_c^{GL}(0)$ is the depairing current density at $T = 0$ K.

The diagram obtained in Ref. [55] for the inhomogeneous states of an HTSC film differs from the inhomogeneous states of a wide LTSC film [28] in that in a layered superconductor the $T = T_1$ state can be both superconducting and resistive. In a wide LTSC film, this can only be a superconducting state.

In Ref. [56] the model proposed to explain the low-temperature nonlinearities of the $I-V$ curves of $YBa_2Cu_3O_x$

films considers the expansion of thermally activated vortex rings to be the reason why superconductors make the transition to the DDM state. According to this model, the flow of current I in a film of depth $d \gg \xi$ gives rise to vortex rings in a plane perpendicular to the current direction. There are two parts to the energy of a vortex ring, the vortex self-energy

$$W(r_L) = 2\pi r_L \left(\frac{\Phi_0}{4\pi\lambda_L}\right)^2 \ln\varkappa - \frac{\Phi_0}{c}\, J\pi r_L^2$$

and the vortex–current interaction energy which plays a role equivalent to that of the Lorentz force. The radius for the appearance of rings varies from the small value $r_L = \xi$ to the large one

$$r_L = r_m \approx \frac{c\Phi_0}{8\pi^2\lambda_L^2 J},$$

which corresponds to $W(r_L) = 0$. The value r_m is a threshold radius at and above which vortex rings are free to expand. As a result, an electric voltage is induced, electrical resistance develops, and energy dissipation appears. The result obtained from this model proved similar to what the model involving vortex–antivortex dipoles in 2D superconductors predicts.

Note that, in a similar manner to film LTSCs, electromagnetic vibrations due to the transport-current-induced vortex motion [57–59], with voltage steps on the $I-V$ curve [60], are observed in HTSC films.

3. DDM states of bulk ceramic HTSC samples as exemplified by $YBa_2Cu_3O_x$ and $Bi_{1.6}Pb_{0.4}Sr_2Ca_2Cu_3O_x$

Ceramic HTSC samples consist of superconducting grains electrically contacted by typical weak links with Josephson junction properties [61]. There are two approaches [62] to explaining energy dissipation: whereas in the first, HTSC samples are considered as superconducting glass [63], the second takes into account the existence of A- and D-vortices in the samples. In the superconducting glass model every grain possesses its own order parameter phase φ. At weak currents I the electrical voltage between ith and jth grains, $V_{ij} = (\hbar/2e)\,\mathrm{d}\varphi/\mathrm{d}t$, arises due to the thermally activated phase 'slip' between them. When $\langle I_i\rangle$, the current averaged over all links, is less than the average critical current $\langle I_{ij}\rangle$, the $I-V$ curve becomes nonlinear due to the influence of thermal fluctuations on the phase slip process [64]. At $\langle I_i\rangle > \langle I_{ij}\rangle$ the $I-V$ curve is linear, with $\mathrm{d}V/\mathrm{d}I \cong R_g$, where R_g is the electrical resistance between grains when they are in the normal state [65]. In 1D and 2D Josephson junctions the effect of the self-field of the current H_i on I_{ij} turns out to be insignificant when they are smaller than a certain critical size [66], whereas for bulk HTSC samples [67], the effect of H_i on I_c is assumed to lead to the low values of $J_c \approx 10^2$ A cm^{-2}.

Models used in the second approach include the vortex motion dynamics in its aspects such as giant flow creep [68], collective flow creep [69], vortex glass [70], etc. The two approaches above are in fact complementary to one another [61]. The study of Ref. [71], for example, along with considering the dissipation due to the flux flow resistivity

$$R_F = \frac{H\Phi_0}{\eta c^2}\,\frac{l_0}{s_0},$$

takes into account the contribution from the microstructure, in the form of all-sample-averaged electrical resistance R_j possessed by the system of percolative links — i.e., by weak link resistances. Here l_0 is the sample length and s_0 is its cross section. The total resistance was $R = R_F + R_j$. Hence, contributions to the total critical current come from the currents I_c^F and I_c^j, where I_c^F is the critical current for vortex penetration into the sample, and I_c^j is the critical value of the current I_{ij}. It is known (see, e.g., Ref. [72] and references therein) that in the temperature range from 77 K to T_c the value of I_c is determined by the pinning force, i.e., $I_c = I_c^F$ and $I_c^F < I_c^j$, whereas at low temperatures the vortex pinning force increases to the point where the critical current is limited by the maximum critical current of the weak links, i.e., $I_c = I_c^j$ and $I_c^F > I_c^j$. From a practical point of view, the temperature range of interest here is 77 K $< T < T_c$, and the percolative contribution to I_c will be ignored in the discussion that follows.

3.1 Penetration of the transport current's magnetic field into a cylindrical type II superconductor

One distinctive property of ceramic HTSCs compared to LTSCs is a large (up to 75%) temperature broadening ΔT_c which occurs in the region of the resistive transition $R(T, H)$ and is due to the features of the vortex state [73]. The temperature interval ΔT_c of the transition $R(T)$ is also broadened as the transport current I increases, both for $H \neq 0$ [74, 75] and $H = 0$ [64, 76–86]. In the latter case, a number of models have been proposed to explain the shape of the $R(T, I)$ curve.

In Ref. [87] a certain statistical distribution was assumed for critical currents in weak links; Ref. [88] considered the statistical distribution of pinning centers; in Refs [89–91], HTSC samples were viewed as consisting of a set of 2D weak superconducting links with the properties of planar superconductors; the analysis of Ref. [76] assumed vortex pairs to exist in intergrain links in the absence of an external field; the model considered in Refs [79, 92] took into account the percolative nature of conduction; and finally, the 'heterophase structure–effective medium' model was proposed in Ref. [93]. These models were deficient in that they offered only a partial explanation of the observed phenomenon.

In addition to the extended temperature region of the current-induced resistive $R(T, I)$ transition to the DDM state, two values of critical current, I_{c1} and I_{c2}, were discovered in Refs [85, 86]. This feature is characteristic of ideal type II superconductors [94–97].

The traditionally held view [34, 94–97] is that an SC to DDM state transition for $I_{c1} < I_c$ results from the motion of magnetic flux in a sample. The dissipation of energy is believed to occur a) because vortices created under the action of the external field H and the self-magnetic field H_i of the transport current I penetrate into the sample, and b) when unstable magnetic flux configurations escape the sample.[1]

In cylindrical, ideal type II superconductors, when $H_i \geqslant H_{c1}$, rings of A-vortices emerge and shrink at the surface and annihilate at the center of the sample, leading to an electrical resistance and the DDM state. The critical current for the onset of resistance or for current instability is

[1] Note Refs [98–100] where the instability of vortex configurations is analyzed disregarding the effect of the surface on the vortex escape process.

[94 – 97]

$$I_{c1} = 0.5crH_{c1}\,, \tag{11}$$

where r is the radius of the cylinder and H_{c1} is the lower critical magnetic field, i.e., the field at which the first vortex ring enters the sample.

The problem of how the self-magnetic field of a transport current penetrates cylindrical type II superconductors has been addressed theoretically in Refs [101 – 103]. In Refs [101, 102], magnetic field structure, magnetic flux, and the free energy of a solid toroidal A-vortex were calculated for an infinite sample, using the results of Londons' theory. Reference [101] served as a starting point for addressing the problem of a vortex ring penetrating a boundary barrier, a problem which was then solved in Refs [103 – 106] using various approaches. Refs [104 – 106] employed a method developed earlier [1] for type I superconductors, to determine the conditions for the penetration of a ringlike A-vortex.

In Refs [104 – 106], magnetic field distribution in a toroidal A-vortex with only one azimuthal field component $h = (0, h(\rho, z), 0)$ in the cylindrical coordinate system (ρ, θ, z) was determined from the solution of Londons' equation for a ring located in the plane $z = 0$,

$$\frac{\partial^2 h}{\partial \rho^2} + \rho^{-1}\,\frac{\partial h}{\partial \rho} - (\rho^{-2} + \lambda_L^{-2})\,h + \frac{\partial^2 h}{\partial z^2} = -\left(\frac{\Phi_0}{\lambda_L^2}\right)\delta(\rho - r_0)\,\delta(z)\,. \tag{12}$$

Here $r_0 < r$ is the radius of the ring.

To proceed further, it was assumed [106] that in exactly the same way that the current of an ideal solenoid does not create a magnetic field in the surrounding space, a closed A-vortex should not create a magnetic field outside the sample (including its surface). The boundary condition of the form $h(\rho = r, z) = 0$ specified in this way made it possible to apply the Hankel transform leading to the following Fourier – Bessel-series solution for Eqn (12):

$$h = \frac{\Phi_0 r_0}{\lambda_L^2 r}\sum_{k=1}^{\infty}\frac{J_1(\gamma_k\rho/r)\,J_1(\gamma_k r_0/r)}{J_2^2(\gamma_k)\left[(\gamma_k^2 + (r/\lambda_L)^2\right]^{0.5}} \times \exp\left\{-|z|\left[\lambda_L^{-2} + \left(\frac{\gamma_k}{r}\right)^2\right]^{0.5}\right\}, \tag{13}$$

where $J_{1,2}$ are Bessel functions of orders 1 and 2 and γ_k are the zeroes of the Bessel function J_1.

From the expression for the vortex free energy,

$$F = \frac{1}{8\pi}\int\left[\mathbf{h}^2 + \lambda_L^2(\mathrm{rot}\,\mathbf{h})^2\right]\mathrm{d}V'$$

(with V' the volume), the free energy of a vortex ring in the cylinder (except to within $\sim\xi$ of the vortex axis) was determined to be

$$F(r_0) = \frac{\Phi_0^2 r_0^2}{4\lambda_L^2}\sum_{k=1}^{\infty}\frac{J_1(\gamma_k r_0/r)\,J_1\left[(r_0 - \xi)/r\right]}{J_2^2(\gamma_k)\left[\gamma_k^2 + (r/\lambda_L)^2\right]^{0.5}}\,. \tag{14}$$

The variation of the free energy $F(r_0)$ of a vortex ring (in units of Φ_0^2/λ_L) is shown in Fig. 7 [106].

Integrating Eqn (12) over the halfplane $-\infty < z < +\infty$, $0 < r < +\infty$ yields [106] an expression for the magnetic flux

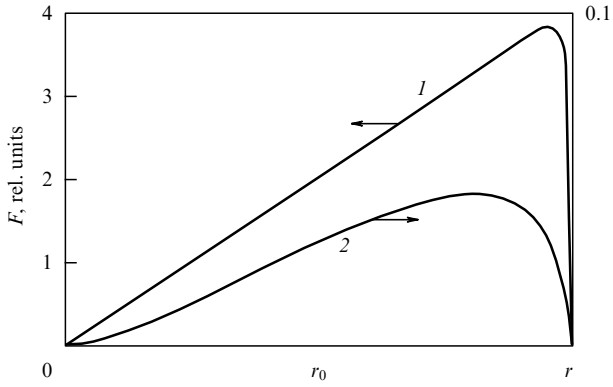

Figure 7. Free energy of a vortex ring inside a superconducting cylinder of radius r, as a function of the ring radius r_0. Free energy is plotted in units of Φ_0^2/λ_L. Curve *1*: $r = 20\,\lambda_L$; curve *2*: $r = 0.5\,\lambda_L$.

in the vortex ring,

$$\Phi(r_0) = \Phi_0\left(\frac{2r_0 r}{\lambda_L}\right) \times \sum_{k=1}^{\infty}\frac{J_1(\gamma_k r_0/r)\left[1 - J_0(\gamma_k)\right]}{J_2^2(\gamma_k)\,\gamma_k\left[\gamma_k^2 + (r/\lambda_L)^2\right]}\,. \tag{15}$$

From Eqn (15) it follows that $\Phi(r_0)$ is zero at the cylinder boundary (Fig. 8), where the circular A-vortex merges with its imaginary image (a concept that acquires a meaning in the limit as $r_0 \to r$), and at $r_0 = 0$, when the vortex shrinks to a point on the cylinder axis.

In Refs [104 – 106] the effect of the barrier on J_c was examined by determining the change in the Gibbs free energy ΔG_c due to vortex ring penetration into a type II superconducting perfectly surfaced cylinder carrying a transport current I. Analogous to the derivation in Ref. [1], the expression for ΔG_c was written in the form

$$\Delta G_c = F - \Delta W_I\,,$$

where $\Delta W_I = (1/c)\,I\Delta\Phi(r_0)$ is the work done by the DC source on the ring entrance. Here $\Delta\Phi(r_0)$ is the magnetic flux which escapes the current source contour when a vortex moves from the cylinder boundary $r_0 = r$ to the position with a radius r_0. Figure 9 shows how the Gibbs free energy $G_c(r_0)$ of a long SC cylinder with $r_0 = 20\lambda_L$ varies with I. $G_c = F$ for

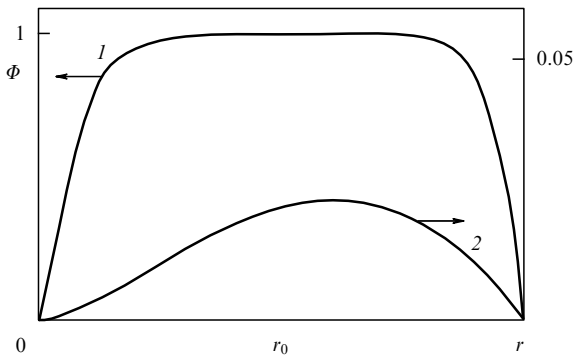

Figure 8. Magnetic flux (in units of Φ_0) flowing through a vortex ring in a long cylinder of radius $r = 20\lambda_L$ (curve *1*) and $r = 0.5\lambda_L$ (curve *2*).

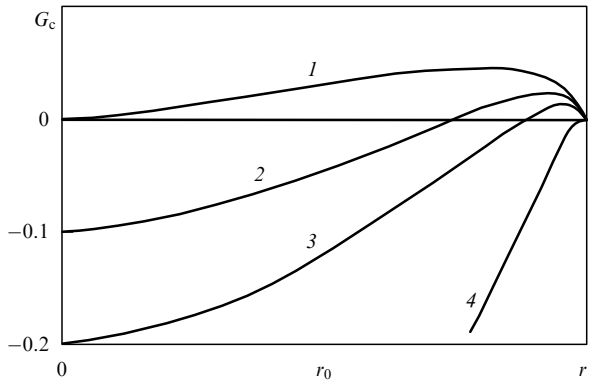

Figure 9. Gibbs free energy of a cylinder containing a vortex ring as a function of current I. $I = 0$ (curve *1*), $I = 0.1I_c$ (*2*), $I = 0.2I_c$ (*3*), and $I = I_c$ (*4*).

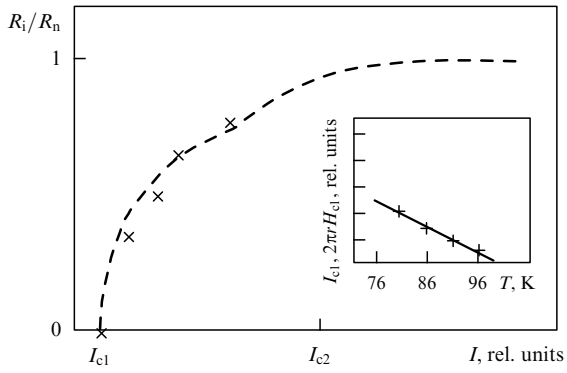

Figure 10. Variation of R_i/R_n with I for $T = 96$ K. Inset: the temperature dependence of I_{c1} or $2\pi rH_{c1}$.

$I = 0$, and the barrier has a width $\sim r$. When $I \geqslant I_c(r)$, the barrier disappears, enabling vortex rings to penetrate spontaneously into the sample. The author of Ref. [106] determined the value of $I_c(r)$ using the criterion $\partial G_c/\partial r_0|_{r_0 \to r} = 0$. The critical current density obtained,

$$J_c = \frac{2\varepsilon_L c}{\Phi_0 \xi} = J_c^{GL},$$

turned out to be independent of r ($\varepsilon_L = (\Phi_0/4\pi\lambda_L)^2$ is the electromagnetic energy of a vortex per unit length). The self-field of the current at the sample surface reaches a value $H_i = H_s = H_c r/\lambda_L$ for $r < \lambda_L$ and $H_i = H_s = H_c$ for $r \gg \lambda_L$, i.e., the transition to the DDM state, as in a type I superconductor with a current, occurs in complete accordance with the Silsby rule — and in disagreement with the previous studies of Refs [94–97], which yield $H_s = H_c/\varkappa$.

On turning off the field the rings shrink and annihilate — except those in the subsurface layer of thickness on the order of λ_L (see Fig. 7), which escape the sample. During the time the vortex rings are escaping an SC sample, the sample restores its diamagnetic properties which were disrupted when it was in the DDM state. To pinpoint this process, the authors of Refs [107, 108] examined the variation with time t of the signal of the real part χ' of the complex dynamic magnetic susceptibility $\chi_{ac} = \chi' + i\chi''$ after the turn-off of transport current in HTSC samples. The idea of the method was that as current flowed through the sample, the value of χ' was varied under the condition [107–110]

$$|\chi'(T, I \neq 0)| < |\chi'(T, I = 0)|.$$

After the current I was turned off, in a certain time the working point pinpointing the signal χ' on the graph plotter moved from the curve $\chi'(T, I \neq 0)$ to the curve $\chi'(T, I = 0)$. By pinpointing the time of this transition at a certain constant temperature $T = T_0$, the authors determined the dependence $\chi'(t)$. Starting from $T = T_c$, after the turn-off of the current I the magnitude of signal χ' remained unchanged for a certain time t_s, and this was taken to be the escape time from the sample for those vortices from the first layer beneath the surface. The effect was observed only in a temperature region where we are in the regime of weakly coupled (rather than isolated) grains [107, 108], where there are D-vortices in the sample. Referring to Fig. 10, the dependence $R(I)$ obtained from curves $R(T, I)$ at 96 K [107] characterizes the change of the DDM state with current I in a sample of $Bi_{1.6}Pb_{0.4}Sr_2Ca_2Cu_3O_x$ with $J_c(T = 77\ \text{K}, H = 0) \approx 10\ \text{A cm}^{-2}$.

Because the temperature range where the effect was observed was one where D-vortices existed, the rings formed by these vortices were supposed [109, 110] to escape the sample. To make things visual, the surface of the HTSC samples was considered as a 2D medium consisting of interconnected bridges of varying thickness, with SC grains as massive electrodes (banks) and weak links as conducting links (bridges) between them. Under certain conditions, D-vortices appear in the weak links due to the influence of the transport current [111], which locate along the circular induction lines of the field H_i and close themselves to form rings near the surface of a HTSC sample.

According to formula (11), $J_c \sim 1/r$, which for $H = 0$ has been confirmed by numerous experiments (see, for example, Refs [112, 113] and Fig. 11). The dependence $J(S)$ changes at $H \neq 0$. It is seen in Fig. 11 that the field weakly affects the critical current density of thin yttrium samples while markedly influencing the current in samples with a large cross section S. This feature is explained by including the effect of the sample size (geometric barrier) — something which was not done in the derivation of Eqn (11) in the case of an ideal type II superconductor in Ref. [34]. If there is a barrier, then [112, 113]

$$j_c = j_0 \quad \text{for} \quad H_i < H_s, \tag{16a}$$

$$j_c = 0 \quad \text{for} \quad H_i > H_s, \tag{16b}$$

where j_c is the local critical current density and j_0 is the local depairing current density. Changing from the local critical field and current to volume ones and averaging over the cross section S of radius r, we obtain as in Ref. [67]

$$J_c = J_c^{GL} \quad \text{for} \quad r < \frac{cH_s}{2\pi j_0}, \tag{17a}$$

$$J_c = \frac{cH_s}{2\pi r} \quad \text{for} \quad r > \frac{cH_s}{2\pi j_0}. \tag{17b}$$

From Eqn (17a) and Refs [104–106] it follows that for $r < 2\lambda_L$, the DDM state does not have enough time to establish itself in an ideal type II superconducting sample with a barrier because the Cooper pair breaking mechanism will do its job before the flow starts. Also, the geometric factor

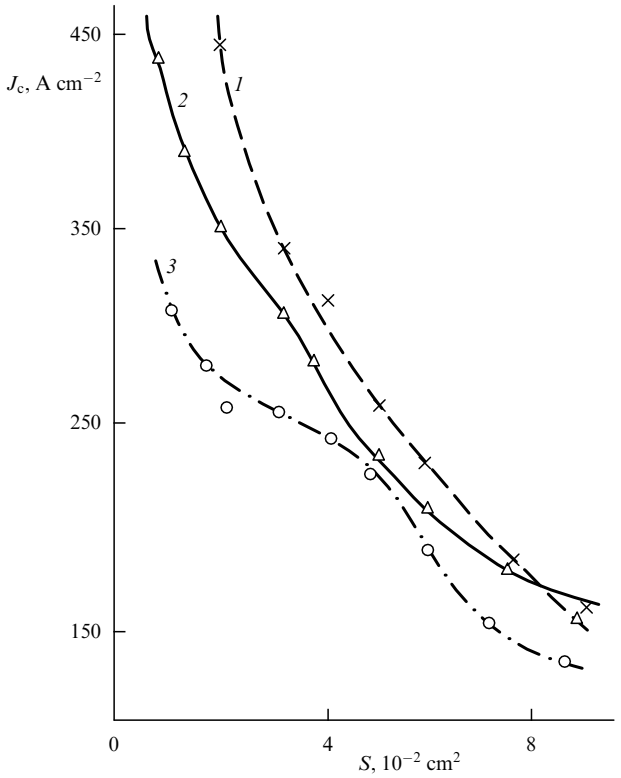

Figure 11. $J_c(H)$ dependence for various external longitudinal fields: $H = 0$ (*1*), $H = 150$ Oe (*2*), and $H = 300$ Oe (*3*) at $T = 77$ K.

will play a role, because vortex rings cannot exist in such a superconductor. For samples with $r \gg \lambda_L$, Eqns (17b) and (11) become identical for $H_s = H_{c1}$.

The conclusions which follow from Eqns (17a) and (17b) are tantamount to stating [106] that due to the influence of current the width of the barrier in bulk samples decreases to $\sim \lambda_L$ for $J_{c1} = \varepsilon_L c/\Phi_0 \lambda_L \ll J_c^{GL}$. Here J_{c1} is the current density which is involved in the defect mechanism for vortex entrance via inhomogeneities $\sim \lambda_L$ and which produces a field equal to H_{c1} at the sample surface. Hence, high values of J_c can be achieved either with samples about 10^{-7} m in size — according to Eqn (17a), or in samples with a large cross section — due to the pinning of vortex rings, which occurs when the radial force F_r of the rings' linear stress is less than the pinning force F_p, where [97]

$$F_r = \frac{\Phi_0 H_{c1}}{4\pi r} \,. \tag{18}$$

In this case, samples are in a critical state, and the model proposed above [112, 113] is a critical state model. It is similar to the models [114, 115] which analyzed samples with a barrier and zero bulk pinning (i.e., with all the pinning concentrated close to the surface) but ignored the effects of transport current on the barrier.

The results obtained from the models of Refs [112, 113] and [67] are identical even though the mechanisms for the transition from the SC to dissipative state are different in the models. Whereas in Ref. [67] this transition is assumed to be due to the direct influence on J_c of the field H_i, in Refs [112, 113] the transition current is defined by the conditions at which vortex rings penetrate into the sample. For example, the effect of the pinning force on vortex dynamics should already be taken into account at 77 K [116]. For 'hard' type II LTSCs, the formation of vortex rings and the dependence $J_c(r)$ were considered in Refs [117, 118].

3.2 DDM states in cylindrical type II superconductors in a magnetic field parallel to the transport current

A magnetic field penetrates a ceramic HTSC sample in a stage-by-stage manner [61]: 1) when $H < H_{c1j}$, the field does not penetrate. Here H_{c1j} is the lower critical field of intergrain links; 2) for $H_{c1j} < H < H_{c2j}$, the field starts penetrating intergrain links in the form of D-vortices (H_{c2j} is the upper critical field of intergrain links; 3) field $H_{c2j} < H < H_{c1g}$ fully penetrates into the intergrain links, H_{c1g} being the lower critical field of a grain; 4) for field $H \geqslant H_{c1g}$, magnetic flux gradually penetrates into the grains in the form of A-vortices. It follows then that the quantities I_{c1} and J_{c1} determined in Section 3.1 for HTSC samples are I_{c1j} and J_{c1j}, respectively.

When a forceless current – field configuration is realized in a superconductor, the external field H parallel to I does not affect the entrance conditions for a vortex ring created by the field H_i. Nor does the transport current I lower the critical field for the penetration of a linear vortex parallel to the cylinder axis [119]. However, varying H and I may lead to vortex configurations closer to the induction lines of the magnetic field — namely to helicoidal vortices [119 – 122], which have thus far been given only a qualitative discussion [98 – 100]. To find out the distribution of the field of a helicoidal vortex in an SC cylinder with a current, Maxwell's equations were solved [119 – 122] combined with Londons' equations with a special right-hand side. The magnetic flux flowing through a helicoidal vortex in the z-direction along the cylinder axis is

$$\Phi_z(r_0) = \Phi_0 \left[1 - \frac{I_0(r_0/\lambda_L)}{I_0(r/\lambda_L)}\right],$$

whatever the helicoid turn length L, whereas this quantity was identically zero for a ring vortex. In the case of a bulk sample, the flux piercing a vortex in the azimuthal direction,

$$\Phi_\perp = \Phi_0 \left[1 - \frac{r_0}{\lambda_L} \, K_1\left(\frac{r_0}{\lambda_L}\right)\right],$$

is the same as for a vortex ring in a bulk sample [103]. Here, $I_k(x)$ and $K_k(x)$ are modified Bessel functions [15].

In Refs [119 – 122] the problem of the energy barrier preventing helicoidal vortices from penetrating or escaping cylindrical SC samples was approached by determining the Gibbs free energy G_h in a similar manner to calculating G_c for a cylinder with a vortex ring. Taking into account the work done by the constant field source, ΔW_H, and that by the dc source, ΔW_I, the expression for G_h can be written [122]

$$\begin{aligned} G_h = {} & \left(\frac{\Phi_0}{4\pi\lambda_L}\right)^2 \sqrt{(1+s^2)} \ln\left[2\frac{(r-r_0)}{\xi}\right] \\ & - \left(\frac{H\Phi_0}{4\pi}\right)\left[1 - \frac{I_0(r_0/\lambda_L)}{I_0(r/\lambda_L)}\right] \\ & \pm \left(\frac{I\Phi_0}{2\pi c L}\right)\left[1 - \frac{r_0 I_1(r_0/\lambda_L)}{r I_1(r/\lambda_L)}\right], \end{aligned} \tag{19}$$

where $s = r/L$ is the tangent of the angle the axis of the helicoid makes with the z axis, and where the upper and lower signs refer to left- and right-hand spiral vortices, respectively. The author of Refs [119 – 122] determined the critical

parameters by using the criterion $\partial G_h/\partial r_0|_{r_0 \to r} = 0$, leading to a critical field for the penetration of a helicoidal vortex at the sample surface, of the form

$$h_{cr}(J,s) = H_c \frac{I_0(r/\lambda_L)}{I_1(r/\lambda_L)} \left[\sqrt{(1+s^2)} - \frac{sJ}{J_L} \right], \qquad (20)$$

where $H_c = \Phi_0/2\sqrt{2}\pi\lambda_L\xi$ and $J_L = cH_c/4\pi\lambda_L$ is the London critical current [95]. The optimum turn length of the spiral, $L = r[(J_L/J)^2 - 1]^{1/2}$, was determined by minimizing h_{cr} with respect to s. On substituting L into Eqn (20), the surface values of the critical current density J_{cr} and the critical field H_{cr} for the penetration of an optimal helicoid were found to be related by [121]

$$\left[\frac{I_1(r/\lambda_L)}{I_0(r/\lambda_L)}\right]^2 \left(\frac{H_{cr}}{H_c}\right)^2 + \left(\frac{J_{cr}}{J_c}\right)^2 = 1\,. \qquad (21)$$

Figure 12a shows, for a sample of $Bi_{1.6}Pb_{0.4}Sr_2Ca_2Cu_3O_x$, the measured $I_c(H)$ dependence typical of granular HTSCs [112]. Such behavior is characteristic of a temperature region close to 77 K. However, starting from 95.1 K and up (Fig. 12b), the $I_c(H)$ dependence changed its form and became similar to that predicted by Eqn (21), suggesting the penetration of helicoidal vortices into the sample. According to Fig. 12b, the relation between I_c and H can be written in the form [112]

$$\frac{I_c^2}{0.013^2} + \frac{H^2}{74^2} = 1\,, \qquad (22)$$

if one considers the curve as part of an ellipse with its center at the origin (the curve is shown dashed in the figure). The reason why the $I_c(H)$ dependence changes its form is that for $T > 95$ K the effective cross section of the Josephson vortex, on the order of λ_j, exceeds the transverse size of the defects, and the pinning forces become so weak that the sample behaves like an ideal type II superconductor.

Relation (21) can also be obtained [112] from the experimental dependence $\varepsilon(H)$ [38] (see Section 2.4) by noting [103] that $I_{cr} = crH_s/2 \propto \varepsilon$.

To learn what vortices exist in a sample and under what conditions they exist, the authors of Ref. [123] determined

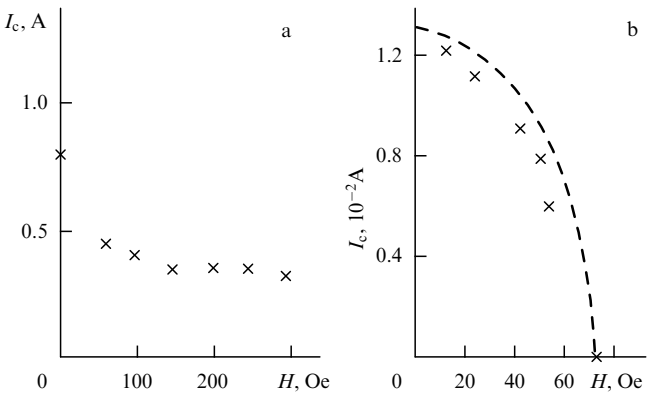

Figure 12. $I_c(H)$ dependence for a ceramic HTSC sample of $Bi_{1.6}Pb_{0.4}Sr_2Ca_2Cu_3O_x$ in a magnetic field parallel to the sample and current: $T = 80.1$ K (a), $T = 95.1$ K (b). The dashed line is the calculated relation (22).

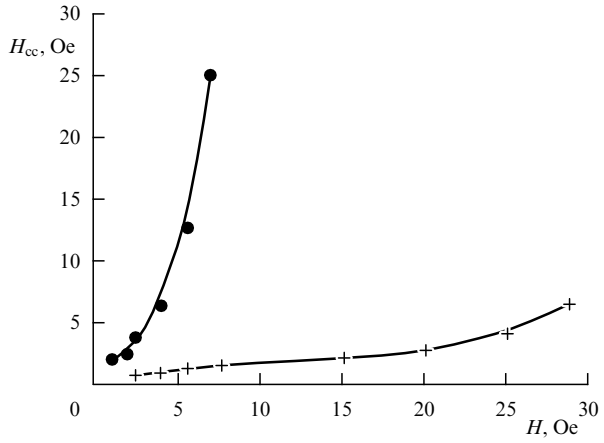

Figure 13. Diagram for the existence of helicoids and circular and linear longitudinal vortices.

the state diagram for helicoids and circular and longitudinal linear vortices. This, according to Eqn (11), requires a knowledge of how T_c^j, the critical temperature of intergrain links, depends on the longitudinal (**H**) and circular transverse ($\mathbf{H}_{cc}$) magnetic fields and their superposition. The studies were made on hollow samples of $Bi_{1.6}Pb_{0.4}Sr_2Ca_2Cu_3O_x$. The circular field was created by a current I_{cc} flowing through a conductor ~ 1 mm in diameter placed in a longitudinal hole in an HTSC sample.

The temperature T_c^j corresponded to the 50% change in the signal $\chi'(T)$ near the SC transition of the weak links [112]. At certain values of the fields **H** and $\mathbf{H}_{cc}$, the curves of the dependences $\chi'(T)$ did or did not shift to lower temperatures by ΔT_c^j. A change in the form of the curves implied that helicoids penetrated the sample. The unchanged form suggested that the superposition of circular and linear vortices existed in the sample. Figure 13 presents a diagram of such states [123]. The curves in the figure determine the upper and lower boundaries of the region where helicoids exits. Outside this region, circular transverse and linear longitudinal D-vortices exist in the sample at **H** and $\mathbf{H}_{cc}$ values about an order of magnitude apart. At comparable values of these fields, helicoids penetrate the samples.

3.3 Effect of circular transverse residual magnetic fields on the DDM transition

In ceramic HTSC samples, along with vortex pinning, the intergrain magnetic induction $\mathbf{B}_j$ determines the value of I_c [124]. Reference [125] argues that the distribution of $\mathbf{B}_j$ in weak links exhibits an inversion of sign after the transport current I_t is turned off. As a result, on repeating the measurement of the current I_c its value increases and the sample makes a transition to the DDM state at a higher transport current $I = I_c$, i.e., the field $\mathbf{H}_i$ created by the current I is sort of mutually compensated by the field which remains in the intergrain links after the current I_t has been turned off. But this statement is at odds with Stokes' theorem. So what does actually happen? The answer depends on the knowledge of the behavior difference between circular magnetic fields in normal versus superconducting cylindrical samples.

When a superconductor with a current is in the normal state, it is known [126] that the circulation of the circular

magnetic field $\mathbf{H}_i$ created by the current is

$$\oint_C \mathbf{H}_i \, d\mathbf{l} = \frac{4\pi}{c} I, \tag{23}$$

where $I = \int \mathbf{J} \, d\mathbf{S}$ is the total current through the cross section surface S enclosed by the contour C. The field $\mathbf{H}_i = 0$ after the current I is turned off. In the superconducting state, the field $\mathbf{H}$ in HTSC samples behaves entirely differently in this case. To verify this, yttrium samples of circular and rectangular cross section [112] were studied in Ref. [123]. At $T = 300$ K, a current I_t was passed through the samples. The samples were then cooled to 77 K, the current I_t was turned off, and I_c was measured using a four-probe scheme. The earth magnetic field was not screened, and the samples were in liquid nitrogen. The value of I_c was determined for two cases, depending on whether I_t and the measuring current I_c were coincident or opposite in direction (curves *1* and *2* in Fig. 14, respectively) [123]. The result obtained confirms the experimental data of Ref. [125]. I_{c0} in Fig. 14 denotes the critical current measured at 77 K and $H = 0$, i.e., upon cooling in a zero magnetic field (ZFC regime). From the way the curves in Fig. 14 appear, there is a residual magnetic field within the yttrium HTSC sample, which affects the value of I_c. The only way this field can be present in a sample is as rings of A-vortices (see Section 3.1) pinned in grains into which they penetrated even at $T = T_c$, when the condition $H_{c1g} \approx 0$ was fulfilled. But the magnetic field $\mathbf{H}_v$ is within a solid circular A-vortex and so cannot be detected outside the SC sample (see Ref. [106], Eqn (16) and Fig. 8) as was done in Ref. [127]. For the field to be present outside the sample the vortex rings must be broken. But this can only happen on some kind of inclusions (inhomogeneities) [128] to which the vortices are attracted with a force $f \propto H_c^2 r_D \xi$ due to a gain in energy [129]. The process of attraction of vortices by inhomogeneities is key to understanding how pinning forces form in both LTSC and HTSC samples [69], as was confirmed experimentally using the decoration technique [130]. Upon a merger with an inhomogeneity, that part of the vortex ring that crosses the inhomogeneity disappears, merging with its imaginary image [129], i.e., the vortex breaks up. The same follows from the analysis of how thin-film LTSC dc transformers work [131].

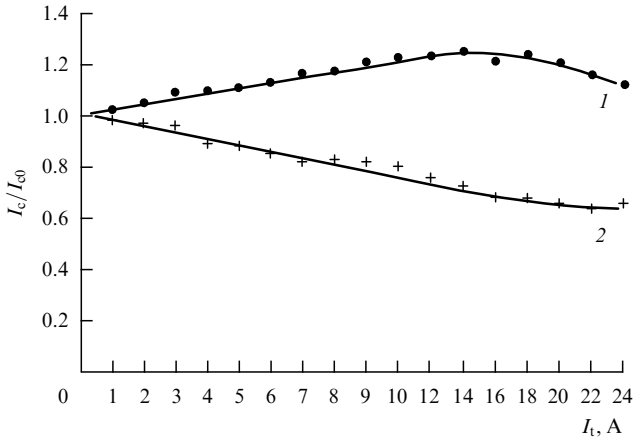

Figure 14. Typical variation of reduced critical currents I_c/I_{c0} with current I_t. *1*, directions of the currents I_t and I coincide; *2*, currents I_t and I are opposite.

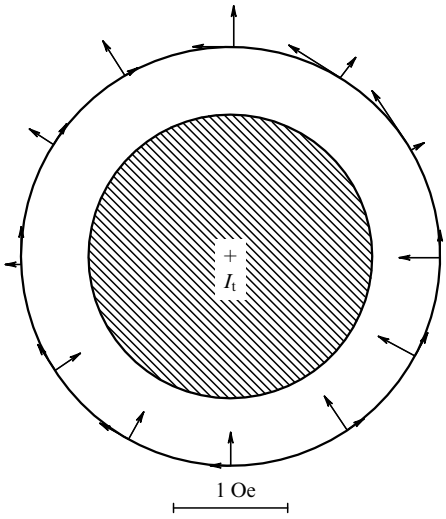

Figure 15. The diagram shows how the parallel and perpendicular components of the circular residual magnetic field are distributed outside a cylindrical yttrium sample (shown dashed) after the current I_t is turned off.

To directly prove the existence of broken A-vortices, the magnitude, form, and distribution of residual circular magnetic fields $\mathbf{H}_{REM}^{out}$ outside yttrium HTSC samples were measured using a standard magnetometer [132, 133]. The sensitivity of the measuring system was 0.01 Oe. In Fig. 15 is shown the distribution of $\mathbf{H}_{REM}^{out}$ in the cross section plane of a sample 4.5×10^{-3} m in diameter and 35×10^{-3} m in length, following the switching off of the current, $I_t = 10$ A, perpendicular to the plane of the figure. Both the magnitude and distribution of the fields remained virtually unchanged along the height of the sample. The magnetic field component parallel to the cylinder directrix was not found to exist, nor was the field at the faces of the cylinder. Figure 16 shows the distribution of the field $\mathbf{H}_{REM}^{out}$ in the 5×10^{-3} m square cross section of a sample 35×10^{-3} m in length. Both the measurement conditions and basic results were the same as

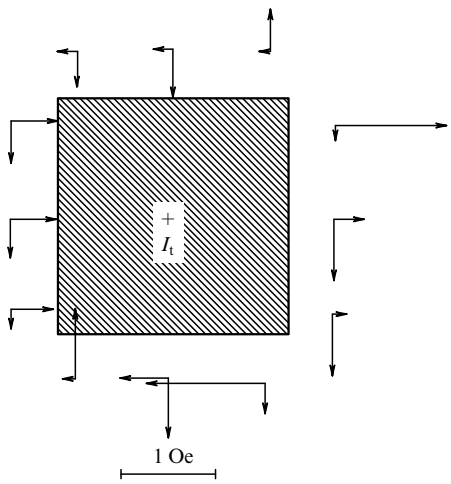

Figure 16. The diagram shows how the parallel and perpendicular components of the circular residual magnetic field are distributed outside a square cross section yttrium sample (shown dashed) after the current I_t is turned off.

for the cylindrical sample. The measured distribution of the field H is similar to the field distribution for a magnet with Eqn (23) fulfilled for $I = 0$ — proving experimentally the absence of singularity in H_v [133]. The reasoning for this is as follows [133]. In a mixed-state type II superconductor, $\mathrm{rot}\,\mathbf{v}_s$ in the neighborhood of a magnetic vortex is nonzero, but what is zero is the circulation along a contour drawn inside and outside the superconductor in the absence of current ($\mathbf{v}_s$ is the velocity of the superconducting (superfluid) electrons that rotate in the vortex). As for superfluid helium in a rotating container, both $\mathrm{rot}\,\mathbf{v}_s$ and the circulation along a contour inside the cylinder are nonzero in the vortex neighborhood (here $\mathbf{v}_s$ is the velocity of the superconducting helium atoms rotating in the vortex). But this is possible only when the region under study is 'spatially' multiply connected [134].

Moreover, it is commonly held [126] that the flux of the vector $\mathbf{H}$ through an arbitrary closed surface S_1 is zero, i.e., $\oint \mathbf{H}\,d\mathbf{S}_1 = 0$. In stating this it is assumed (although never mentioned) that the region under study is 'spatially' simply connected. After that the conclusion is drawn based on the Gauss theorem that $\mathrm{div}\,\mathbf{H} = 0$ and that the magnetic field has neither sources nor sinks for magnetic charges. But in 'spatially' multiconnected regions — even in ones with point singularities — the Gauss theorem is not valid [135], and $\mathrm{div}\,\mathbf{H} \neq 0$. Hence, from the magnetism point of view, 'spatially' multiconnected regions do allow the existence of magnetic monopoles.

To return to inhomogeneous superconductors, it can be argued that vortex rings break up when being attracted by and crossing pores and non-superconducting inclusions of size $r_D > \lambda_L$ [136]. The magnetic fields H_v of the vortices crossing non-superconducting inclusions are dissipated through the ring breakup regions. The induction lines corresponding to these fields do not break up but deform in a complicated way. The dissipated magnetic fields existing in the intergrain space of weak links outside the vortices' pinned portions penetrate into the grains to a depth λ_L and partially escape the sample. Figure 17 shows what the magnetic field distribution inside an inhomogeneity (pore) with $r_D > \lambda_L$ in the breakup region of a vortex ring should be like if the vortex distribution in a grain is taken to be that in a mesoscopic disk-like sample [137, 138]. The existence, in mesoscopic cylindrical samples, of vortices with a magnetic flux $\Phi < \Phi_0$ was predicted long ago in Refs [139 – 141]. In grains of sizes 10^{-5} – 10^{-6} m, as in mesoscopic samples [137, 138], vortices with a magnetic flux $\Phi < \Phi_0$ can exist. If the grain separation exceeds λ_L, the magnetic induction lines of the dissipation field can even close themselves around the grains. The small values of $\mathbf{H}^{out}_{REM}$ indicate that only a small fraction of the magnetic field $\mathbf{H}_v$ is dissipated, whereas the main part of it, $\mathbf{H}^{in}_{REM}$, remains within the sample, coinciding in direction with $\mathbf{H}_i$. Nor does $\mathbf{B}_j$ change its direction and sign after the transport current is turned off.

The result obtained, although due to a different effect, is reminiscent of how a magnetic-field cooled superconducting sphere with a perfect conductivity becomes a magnetic dipole after a magnetic field is turned off.

Thus, the $I_c(I_t)$ dependences in Fig. 14 can be explained [123] as resulting from the interaction between the broken rings of A-vortices (A-rings) that are trapped in the sample and the rings of D-vortices (D-rings) penetrating the sample. For the interaction between grain-pinned solid A-vortices and D-vortices penetrating a sample at an external field $H \neq 0$, see Ref. [142].

The way the presence of the field $\mathbf{H}^{in}_{REM}$ affects the penetration of D-rings is as follows. The pinned broken A-rings repel the incoming D-rings of the same sign. These latter must overcome this repulsion force to penetrate the sample, and it is for this exact reason that a current additional to I_{c0} is needed (curve *1* in Fig. 14). The entrance of D-rings of opposite sign to the pinned broken A-rings is facilitated by their mutual attraction, so the critical current will be lower than I_{c0} in this case (curve *2* in Fig. 14). The force acting on the penetrating D-vortices is [123] (see Section 3.1)

$$F = F_r \pm \Delta F = F_r \pm \Phi_0 \frac{\Delta H}{4\pi r}\,, \tag{24}$$

where ΔH is the difference between the magnetic fields the currents $I_c(I_t)$ and I_{c0} generate at the sample surface. For rings of the same sign, the plus sign is taken, with the minus sign taken otherwise. Figure 18 shows how the additional force $|\Delta F|$ exerted on a D-ring entering an yttrium HTSC sample varies with I_t — or in fact with the residual magnetic field H^{in}_{REM}. The change in the nature of the $I_c(I_t)$ dependence for $I_t > 10$ A (see Fig. 14) is presumably due to Joule heating effects.

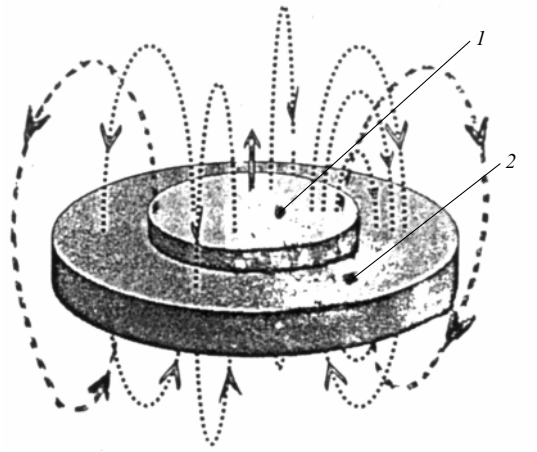

Figure 17. Dissipated magnetic field H_v of a vortex (*1*) in a grain (*2*) viewed as a mesoscopic sample.

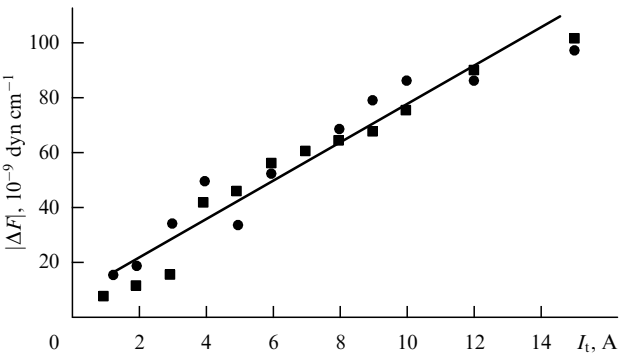

Figure 18. Variation of additional force $|\Delta F|$ with current I_t for coincident (circles) and opposite (squares) I_t and I directions.

3.4 Effect of longitudinal residual magnetic fields on the DDM transition

In HTSC samples, dissipation fields should also exist for linear, pinned broken A-vortices created by an external field **H** parallel to the cylinder axis and current **I** — this is what critical current hysteresis dependent on the magnetic prehistory of a sample suggests (see, for example, Ref. [143]). In Refs [123, 144], critical currents in yttrium and bismuth – lead HTSC samples were measured at 77 K in the ZFC and FC (cooling in a field **H**) regimes to study the effect of the residual magnetic field $\mathbf{H}_{\rm REM}$ on the value of $I_{\rm c}$. In the first case the critical current measured in the growing field **H** was denoted by $I_{1\rm c}(H)$, and that measured in a decreasing field by $I_{2\rm c}(H)$. The critical current $I_{3\rm c}(H)$ was determined after the turn-on and turn-off of the field **H**. For FC measurements, when a sample was cooled to 77 K in a field **H** which was not turned off, a critical current $I_{4\rm c}(H)$ was determined. The critical current $I_{5\rm c}(H)$ was measured in the residual magnetic field when the field was turned off on cooling the sample to 77 K. If the field was then turned on again, the critical current $I_{6\rm c}(H)$ was determined. Figure 19 presents typical data obtained in one of the yttrium samples. The hysteretic behavior of the currents $I_{1\rm c}$ and $I_{2\rm c}$ resulted from the magnetic field being trapped in grains for $H = 300$ Oe $> H_{\rm c1g}$. The condition $I_{3\rm c} = I_{\rm c0}$ implied that after the field **H** was turned off the field that remained in the sample $\mathbf{H}^{\rm in}_{\rm REM} < \mathbf{H}_{\rm c1j}$. The inequality $I_{1\rm c} < I_{4\rm c}$ confirms the existence in the sample of the field $\mathbf{H}^{\rm in}_{\rm REM}$ which is created by the broken vortices and which compensates the field **H**.

In FC measurements to $H < 75$ Oe the equality $I_{6\rm c} = I_{4\rm c}$ implied that $H_{\rm TRAP} = H_{\rm REM}$, where $H_{\rm TRAP}$ is the field which was trapped by the sample and $H_{\rm REM}$ is that which remained in the sample after the external field **H** was turned off. An increase in the field **H** led to the fulfillment of the condition $I_{6\rm c} < I_{4\rm c}$, and hence $H_{\rm REM}$ became less than $H_{\rm TRAP}$ due to the effect of the grains' Bean – Livingston barrier on the properties of the vortices.

In summary then, the critical currents (or more precisely, currents for the SC to DDM state transition) depend on the residual field in the sample $H^{\rm j}_{\rm REM}$, where $H^{\rm j}_{\rm REM}$ is the magnetization of intergrain links to which the dissipation fields $H_{\rm v}$ of broken vortices make a contribution. In Refs [123, 144] the equality of the effective magnetic fields and currents measured in different regimes (see Fig. 19) was employed to determine the trapped ($H^{\rm j}_{\rm TRAP}$) and residual

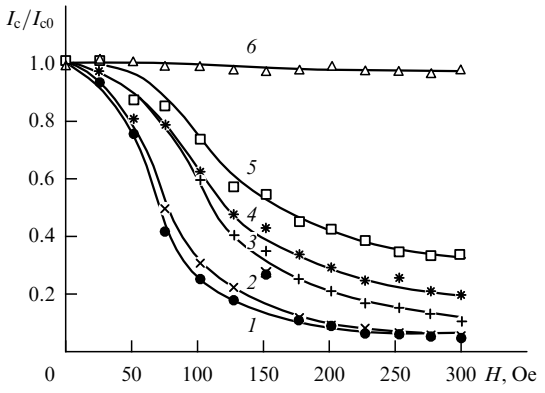

Figure 19. Variation of reduced critical currents $I_{\rm c}/I_{\rm c0}$ with the external longitudinal magnetic field H: $I_{1\rm c}(H)$, curve *1*; $I_{2\rm c}(H)$ (*2*); $I_{6\rm c}(H)$ (*3*); $I_{4\rm c}(H)$ (*4*); $I_{5\rm c}(H)$ (*5*); and $I_{3\rm c}(H)$ (*6*).

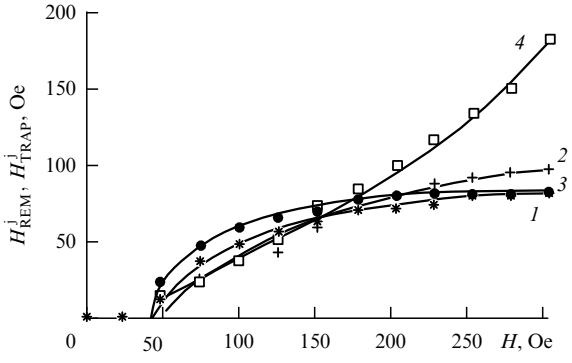

Figure 20. Variation of $H^{\rm j}_{\rm REM}$ (curves *1–3*) and $H^{\rm j}_{\rm TRAP}$ (*4*) with field H. Curves *1*, *2*, and *3* are calculated, respectively, by methods 1, 2 and graphically (see the text).

($H^{\rm j}_{\rm REM}$) magnetic fields in the intergrain region. The field $H^{\rm j}_{\rm REM}$ was determined by two different methods (Fig. 20):

1) by equating the currents $I_{1\rm c}$ and $I_{5\rm c}$, which yields $H^{\rm j}_{\rm REM} \cong H_1$, where H_1 is the field in which the yttrium sample was when its $I_{1\rm c}$ was measured;

2) from the comparison of the currents $I_{1\rm c}$ and $I_{6\rm c}$ it follows that $H^{\rm j}_{\rm REM} \cong H_6 - H_1$, where H_6 is the field in which the sample was when $I_{6\rm c}$ was measured.

These values were compared with the $H^{\rm j}_{\rm REM}$ obtained graphically — directly from the maxima observed in the $I_{\rm c}(H)$ dependences for the field **H** maximally compensated by $\mathbf{H}^{\rm j}_{\rm REM}$.

The field $H^{\rm j}_{\rm TRAP}$ trapped in the intergrain space cannot be determined experimentally, and its value was calculated [121, 141] using the equalities $I_{4\rm c} = I_{1\rm c}$ and $H_{\rm eff4} = H_{\rm eff1}$. Then $H^{\rm j}_{\rm TRAP} \cong H_4 + H_1$, where H_4 is the field in which the sample was when $I_{4\rm c}$ was measured. Figure 20 shows the dependences $H^{\rm j}_{\rm REM}(H)$ and $H^{\rm j}_{\rm TRAP}(H)$ obtained on weak-current samples with $J\,(T = 77\ {\rm K},\ H = 0) < 5\ {\rm A\ cm^{-2}}$.

4. Conclusions

The title theme has become increasingly topical in recent years in light of the practical applications of ceramic HTSC samples as conducting wires, etc. Many of the transport properties of type II superconductors depend significantly on the flow of magnetic flux in the material. Of this entire area of research — the dynamics of vortices and domains of the normal phase — only a small fraction, namely the magnetic flux flow due to transport current — is covered in this review. The studies performed led to a clear understanding of things such as:

1) the 'giant Josephson generation' of electromagnetic vibrations in LTSC films;

2) DDM states resulting from the penetration and motion of D-rings in ceramic HTSC samples at small currents, compared to the depairing current;

3) the dynamics of vortex rings and its magnetic field dependence;

4) current hysteretic loops and the effects of external magnetic fields on their shape;

5) vortices broken at inhomogeneities and the effect of their magnetic field (including the residual field) on the electrical and magnetic properties of ceramic HTSC samples.

The authors would like to thank V Ya Yampol'skiĭ for a discussion of a number of problems reviewed.

References

1. Huebener R P *Magnetic Flux Structures in Superconductors* (Berlin: Springer-Verlag, 1979) [Translated into Russian (Moscow: Mashinostroenie, 1984)
2. Mints R G, Rakhmanov A L *Neustoĭchivosti v Sverkhprovodnikakh* (Instabilities in Superconductors) (Moscow: Nauka, 1984)
3. Bednorz J G, Müller K A *Z. Phys. B* **64** 189 (1986)
4. Cohen R W, Abeles B *Phys. Rev.* **168** 444 (1968)
5. Khirnyĭ V F, Ph. D. Thesis (Donetsk: Donetsk Physico-Technical Institute of the Academy of Sciences of the Ukrainian SSR, 1981) p. 143
6. Galkin A A, Ivanchenko Yu M, Khirnyi V F *Fiz. Tverd. Tela* **20** 1237 (1978)
7. Ivanchenko Yu M, Khirnyi V F *Fiz. Nizk. Temp.* **4** 969 (1978)
8. Ivanchenko Yu M, Khirnyi V F, Mikheenko P N *Zh. Eksp. Teor. Fiz.* **77** 952 (1979) [*Sov. Phys. JETP* **50** 479 (1979)]
9. Ivanchenko Yu M, Mikheenko P N, Khirnyi V F *Zh. Eksp. Teor. Fiz.* **80** 161 (1981) [*Sov. Phys. JETP* **53** 81 (1981)]
10. Medvedev Yu V, Khirnyi V F *Fiz. Tverd. Tela* **26** 1163 (1984) [*Sov. Phys. Solid State* **26** 705 (1984)]
11. Ivanchenko Yu M, Medvedev Yu V, Mikheenko P N, Khirnyi V F, Preprint No. 82-38 (Donetsk: Donetsk Physico-Technical Institute of the Academy of Sciences of the Ukrainian SSR, 1982)
12. Kupriyanov M Yu, Likharev K K *Fiz. Tverd. Tela* **16** 2829 (1974) [*Sov. Phys. Solid State* **16** 1835 (1975)]
13. Bean C P, Livingston J D *Phys. Rev. Lett.* **12** 14 (1964)
14. Likharev K K *Izv. Vyssh. Uchebn. Zaved. Radiofiz.* **14** 909, 919 (1971) [*Radiophys. Quantum Electron.* **14** 714, 722 (1972)]
15. Gradshtein I S, Ryzhik I P *Tablitsy Integralov, Summ, Ryadov i Proizvedeniĭ* (Table of Integrals, Series, and Products) (Moscow: Nauka, 1971) p. 385 [Translated into English (New York: Academic Press, 1980)]
16. Rhoderick E H, Wilson E M *Nature* **194** 1167 (1962)
17. Larkin A I, Ovchinnikov Yu N *Zh. Eksp. Teor. Fiz.* **61** 1221 (1971) [*Sov. Phys. JETP* **34** 651 (1972)]
18. Andratskii V P et al. *Zh. Eksp. Teor. Fiz.* **65** 1591 (1973) [*Sov. Phys. JETP* **38** 794 (1974)]
19. Ginzburg V L *Dokl. Akad. Nauk SSSR* **118** 464 (1958) [*Sov. Phys. Dokl.* **3** 102 (1958)]
20. Gubankov V N, Likharev K K, Pavlov N B *Fiz. Tverd. Tela* **14** 3186 (1972) [*Sov. Phys. Solid State* **14** 2721 (1973)]
21. Pearl J *Appl. Phys. Lett.* **5** 65 (1964)
22. Josephson B D *Adv. Phys.* **14** 419 (1965)
23. Huebener R P *Phys. Rep.* **13** 143 (1974)
24. Artemenko S N, Volkov A F *Usp. Fiz. Nauk* **128** 3 (1979) [*Sov. Phys. Usp.* **22** 295 (1979)]
25. Ivanchenko Yu M, Medvedev Yu V, Mikheenko P N, Preprint No. 82-37 (Donetsk: Donetsk Physico-Technical Institute of the Academy of Sciences of the Ukrainian SSR, 1982)
26. Ivanchenko Yu M, Mikheenko P N *Zh. Eksp. Teor. Fiz.* **82** 488 (1982) [*Sov. Phys. JETP* **55** 281 (1982)]
27. Ivanchenko Yu M, Medvedev Yu V, Mikheenko P N *Fiz. Tverd. Tela* **25** 763 (1983) [*Sov. Phys. Solid State* **25** 436 (1983)]
28. Artemov A N, Medvedev Yu V *Fiz. Tverd. Tela* **45** 385 (2003) [*Phys. Solid State* **45** 409 (2003)]
29. Ivanchenko Yu M, Mikheenko P N, Yuzhelevskii Ya I *Pis'ma Zh. Eksp. Teor. Fiz.* **45** 483 (1987) [*JETP Lett.* **45** 618 (1987)]
30. Pashitskiĭ E A *Osnovy Teorii Sverkhprovodimosti* (Fundamentals of the Theory of Superconductivity) (Kiev: Vishcha Shkola, 1985)
31. Besuglyi A I, Shklovskij V A *J. Low Temp. Phys.* **57** 227 (1984)
32. Eru I I, Peskovatskii S A, Poladich A V *Fiz. Tverd. Tela* **21** 2004 (1979)
33. Khirnyi V F *Fiz. Tverd. Tela* **41** 577 (1999) [*Phys. Solid State* **41** 516 (1999)]
34. de Gennes P G *Superconductivity of Metals and Alloys* (New York: W.A. Benjamin, 1966) [Translated into Russian (Moscow: Mir, 1968)]
35. Maki K, in *Superconductivity* Vol. II (Ed. R D Parks) (New York: M. Dekker, 1969) Pt. 18, p. 1035
36. Abrikosov A A, Gor'kov L P *Zh. Eksp. Teor. Fiz.* **39** 1781 (1960) [*Sov. Phys. JETP* **12** 1243 (1960)]
37. Gulyan A M, Zharkov G F *Sverkhprovodniki vo Vneshnikh Polyakh. Neravnovesnye Yavleniya* (Moscow: Nauka, 1990); Gulian A M, Zharkov G F *Nonequilibrium Electrons and Phonons in Superconductors*: Selected Topics in Superconductivity (New York: Kluwer Acad./Plenum, 1999)
38. Douglass D, Falikov L, in *Progress in Low Temperature Physics* Vol. 4 (Ed. C Gorter) (New York: J. Wiley, 1964) [Translated into Russian: in *Sverkhprovodimost'* (Superconductivity) (Moscow: Nauka, 1967) p. 9]
39. Churilov G E et al. *Fiz. Nizk. Temp.* **15** 994 (1989) [*Sov. J. Low Temp. Phys.* **15** 550 (1989)]
40. Moskvin S I *Fiz. Nizk. Temp.* **11** 878 (1985) [*Sov. J. Low Temp. Phys.* **11** 483 (1985)]
41. Dmitrenko I M *Fiz. Nizk. Temp.* **22** 849 (1996) [*Low Temp. Phys.* **22** 648 (1996)]
42. Berezinskii V L *Zh. Eksp. Teor. Fiz.* **61** 1144 (1971) [*Sov. Phys. JETP* **34** 610 (1972)]
43. Kosterlitz J M, Thouless D J *J. Phys. C: Solid State Phys.* **6** 1181 (1973)
44. Artemenko S N, Kruglov A N *Phys. Lett. A* **143** 485 (1990)
45. Buzdin A I, Feinberg D *J. Phys.* (Paris) **51** 1971 (1990)
46. Glazman L I, Koshelev A E *Zh. Eksp. Teor. Fiz.* **97** 1371 (1990) [*Sov. Phys. JETP* **70** 774 (1990)]
47. Minnhagen *Rev. Mod. Phys.* **59** 1001 (1987)
48. Artemov A N, Martynovich A Yu *Zh. Eksp. Teor. Fiz.* **109** 265 (1996) [*JETP* **82** 140 (1996)]
49. Lawrence W E, Doniach S, in *Proc. of the 12th Intern. Conf. on Low Temperature Physics, Kyoto, 1970* (Ed. E Kanda) (Tokyo: Kcegaku, 1971) p. 361
50. Artemov A N et al. *Fiz. Tekhn. Vys. Davl.* **11** 110 (2001)
51. Jensen H J, Minnhagen P *Phys. Rev. Lett.* **66** 1630 (1991)
52. Maksimov I L, Vodolazov D Yu *Pis'ma Zh. Tekh. Fiz.* **24** (21) 1 (1998) [*Tech. Phys. Lett.* **24** 829 (1998)]
53. Fix A Sh et al. *IEEE Trans. Appl. Supercond.* **AS-3** 1608 (1993)
54. Grishin A M, Medvedev Yu V, Nikolaenko Yu M *Fiz. Tverd. Tela* **41** 1377 (1999) [*Phys. Solid State* **41** 1260 (1999)]
55. Artemov A N, Medvedev Yu V *Fiz. Nizk. Temp.* **28** 349 (2002) [*Low Temp. Phys.* **28** 242 (2002)]
56. Jiang H et al. *Phys. Rev. B* **45** 3048 (1992)
57. Jung G et al. *Appl. Phys. Lett.* **54** 2355 (1989)
58. Amatuni L E et al. *Physica B* **173** 316 (1991)
59. Amatuni L E et al. *Pis'ma Zh. Eksp. Teor. Fiz.* **50** 355 (1989) [*JETP Lett.* **50** 385 (1989)]
60. Kupriyanov M Yu, Likharev K K *Usp. Fiz. Nauk* **160** (5) 49 (1990) [*Sov. Phys. Usp.* **33** 340 (1990)]
61. Meilikhov E Z *Sverkhprovodimost': Fiz., Khim., Tekhn.* **2** (9) 5 (1989)
62. Clem J R *Physica C* **153–155** 50 (1988)
63. Ebner C, Stroud D *Phys. Rev. B* **31** 165 (1985)
64. Blackstead H A *J. Supercond.* **5** 67 (1987)
65. Tiernan W M, Hallock R B *Phys. Rev. B* **43** 10508 (1991)
66. Vinokur V M, Koshelev A E *Zh. Eksp. Teor. Fiz.* **97** 976 (1990) [*Sov. Phys. JETP* **70** 547 (1990)]
67. Dersch H, Blatter G *Phys. Rev. B* **38** 11391 (1988)
68. Yeshurun Y, Malozemoff A P *Phys. Rev. Lett.* **60** 2202 (1988)
69. Blatter G et al. *Rev. Mod. Phys.* **66** 1125 (1994)
70. Fisher M P A *Phys. Rev. Lett.* **62** 1415 (1989)
71. Mocaër P et al. *J. Less Common Metals* **164–165** 1055 (1990)
72. Plecháček V et al. *Physica C* **225** 361 (1994)
73. Sergeeva G G *Fiz. Nizk. Temp.* **18** 797 (1992) [*Sov. J. Low Temp. Phys.* **18** 561 (1992)]
74. Ikeda R, Ohmi T, Tsuneto T *J. Phys. Soc. Jpn.* **58** 1377 (1989)
75. Gammel P L et al. *Phys. Rev. Lett.* **61** 1666 (1988)
76. Koch R H et al. *Phys. Rev. Lett.* **63** 1511 (1989)
77. Takamura S, Hoshiya T, Aruga T *Appl. Phys. Lett.* **56** 1582 (1990)
78. Bowley R M et al. *Physica C* **159** 51 (1989)
79. Göldschmidt D *Phys. Rev. B* **39** 2372 (1989)
80. Wördenweber R, Heinemann K, Freyhardt H C *Cryogenics* **28** 694 (1988)
81. Goldschmidt D *Phys. Rev. B* **39** 9139 (1989)
82. Kardiwarman I, Suzuki M, Burr C R *J. Phys.: Condens. Matter* **1** 8491 (1989)
83. Veira J A et al. *J. Less Common Metals* **151** 77 (1989)
84. Paracchini C *Solid State Commun.* **74** 1113 (1990)

85. Frenkel A et al. *J. Appl. Phys.* **67** 3767 (1990)
86. Hascicek Y S, Testardi L R *IEEE Trans. Magn.* **MAG-27** 1186 (1991)
87. Bradley R M et al. *J. Phys. A: Math. Gen.* **20** L911 (1987)
88. Plammer C J G, Evetts J E *IEEE Trans. Magn.* **MAG-23** 1179 (1987)
89. Resnick D J et al. *Phys. Rev. Lett.* **47** 1542 (1981)
90. Hebard A T, Fiory A T *Phys. Rev. Lett.* **50** 1603 (1983)
91. Fiory A T, Hebard A F, Glaberson W I *Phys. Rev. B* **28** 5075 (1983)
92. Prester M et al. *Phys. Rev. B* **49** 6967 (1994)
93. Daunov M I, Buttaev M S, Magomedov A B *Sverkhprovodimost': Fiz., Khim., Tekh.* **5** 73 (1992)
94. Saint-James D, Sarma G, Thomas E J *Type II Superconductivity* (Oxford: Pergamon Press, 1969) [Translated into Russian (Moscow: Mir, 1970)]
95. Tinkham M *Introduction to Superconductivity* (New York: McGraw-Hill, 1975) [Translated into Russian (Moscow: Atomizdat, 1980)]
96. Ullmaier H *Irreversible Properties of Type II Superconductors* (Berlin: Springer-Verlag, 1975)
97. Campbell A M, Evetts J E *Critical Currents in Superconductors* (London: Taylor and Francis, 1972) [Translated into Russian (Moscow: Mir, 1975)]
98. Clem J R *Phys. Rev. Lett.* **38** 1425 (1977)
99. Brandt E H *Phys. Lett. A* **79** 207 (1980)
100. Brandt E H *Phys. Rev. B* **25** 5756 (1982)
101. Kozlov V A, Samokhvalov A V *Pis'ma Zh. Eksp. Teor. Fiz.* **53** 150 (1991) [*JETP Lett.* **53** 158 (1991)]
102. Kozlov V A, Samokhvalov A V *Physica C* **213** 103 (1993)
103. Gordion I M *Sverkhprovodimost': Fiz., Khim., Tekh.* **5** 1993 (1992) [*Supercond.: Phys., Chem., Technol.* **5** 1896 (1992)]
104. Genenko Yu A *Physica C* **215** 343 (1993)
105. Genenko Yu A, in *Applied Superconductivity: Proc. of the Eur. Conf., EUCAS93, Göttingen, Oct. 4 – 9, 1993* Vol. 1 (Ed. H C Freyhardt) (Oberursel: Informationgesellschaft Verlag, 1993) p. 733
106. Genenko Yu A *Phys. Rev. B* **49** 6950 (1994)
107. Khirnyi V F, Seminozhenko V P, Kozlovskii A A, Grinchenko Yu A *Fiz. Nizk. Temp.* **20** 774 (1994) [*Low Temp. Phys.* **20** 607 (1994)]
108. Seminozhenko V P, Khirnyi V F, Grinchenko Yu A, Kozlovskii A A *Sverkhprovodimost': Fiz., Khim., Tekh.* **6** 2010 (1993) [*Supercond.: Phys., Chem., Technol.* **6** (1993)]
109. Seminozhenko V P et al. *Fiz. Tekhn. Vys. Davl.* **3** 147 (1993)
110. Grinchenko Yu A et al. *Sverkhprovodimost': Fiz., Khim., Tekhn.* **5** 2064 (1992) [*Supercond.: Phys., Chem., Technol.* **5** 1960 (1992)]
111. Likharev K K *Usp. Fiz. Nauk* **127** 185 (1979) [*Sov. Phys. Usp.* **22** 67 (1979)]
112. Khirnyi V F, Seminozhenko V P, Kozlovskii A A *Fiz. Tverd. Tela* **38** 2951 (1996) [*Phys. Solid State* **38** 1614 (1996)]
113. Khirnyi V F, Seminozhenko V P, Kozlovsky A A *Funct. Mater.* **3** 179 (1996)
114. Clem J R, in *Proc. of the 13th Conf. on Low Temperature Physics* Vol. 3 (Ed. K D Timmerhaus, W J O'Sullivann, E F Hammel) (New York: Plenum, 1974) p. 102
115. Burlachkov L *Phys. Rev. B* **47** 8056 (1993)
116. Khirnyi V F et al. *Funct. Mater.* **3** 187 (1996)
117. Koppe H *Phys. Status Solidi* **17** K229 (1966)
118. Ulmaier H A, Kernohan R H *Phys. Status Solidi* **17** K233 (1966)
119. Genenko Yu A *Pis'ma Zh. Eksp. Teor. Fiz.* **59** 807 (1994) [*JETP Lett.* **59** 841 (1994)]
120. Genenko Yu A *Physica C* **235 – 240** 2709 (1994)
121. Genenko Yu A *Phys. Rev. B* **51** 3686 (1995)
122. Genenko Yu A *Fiz. Nizk. Temp.* **22** 1272 (1996) [*Low Temp. Phys.* **22** 967 (1996)]
123. Kozlovskiĭ A A, Khirnyĭ V *Fiz. Tverd. Tela* **42** 1780 (2000) [*Phys. Solid State* **42** 1825 (2000)]
124. Evetts J E, Glowacki B A *Cryogenics* **28** 641 (1988)
125. Zhukov A A, Moshchalkov V V *Sverkhprovodimost': Fiz., Khim., Tekh.* **4** 850 (1991) [*Supercond.: Phys., Chem., Technol.* **4** 759 (1991)]
126. Levich V G *Kurs Teoreticheskoĭ Fiziki* (A Course in Theoretical Physics) Vol. 1 (Moscow: Fizmatgiz, 1962) [Translated into English: *Theoretical Physics*; *an Advanced Text* Vol. 1 (Amsterdam: North-Holland Publ. Co., 1970)]
127. Yahara À, Matsuba H *Cryogenics* **29** 405 (1989)
128. Lifshitz E M, Pitaevskiĭ L P *Statisticheskaya Fizika* (Statistical Physics) Pt. 2 (Moscow: Nauka, 1978) [Translated into English (Oxford: Pergamon Press, 1980)]
129. Abrikosov A A *Osnovy Teorii Metallov* (Fundamentals of the Theory of Metals) (Moscow: Nauka, 1987) [Translated into English (Amsterdam: North-Holland, 1988)]
130. Jou C J et al. *Appl. Phys. Lett.* **52** 326 (1988)
131. Clem J R *Phys. Rev. B* **12** 1742 (1975)
132. Khirnyĭ V F, Kozlovskiĭ A A, Deineka T G *Vopr. Atom. Nauki Tekhn. Ser. 5. Vakuum, Chistye Metally, Sverkhprovodniki* (11) 46 (2000)
133. Khirnyĭ V F, Kozlovskiĭ A A *Fiz. Tverd. Tela* **43** 2117 (2001) [*Phys. Solid State* **43** 2209 (2001)]
134. Feynman R P, in *Progress in Low Temperature Physics* Vol. 1 (Ed. C Gorter) (Amsterdam: North-Holland, 1964) p. 17
135. Fikhtengol'ts G M *Kurs Differentsial'nogo i Integral'nogo Ischisleniya* (A Course in Differential and Integral Calculus) Vol. 3 (Moscow: Nauka, 1966)
136. Seminozhenko V P et al. *Funct. Mater.* **1** 19 (1994)
137. Geim A K et al. *Nature* **407** 55 (2000)
138. Milosevic M V, Yampolskii S V, Peeters F M *Phys. Rev. B* **66** 024515 (2002); cond/mat 0107410
139. Bardeen J *Phys. Rev. Lett.* **7** 162 (1961)
140. Keller J B, Zumino B *Phys. Rev. Lett.* **7** 164 (1961)
141. Ginzburg V L *Zh. Eksp. Teor. Fiz.* **42** 299 (1962) [*Sov. Phys. JETP* **15** 207 (1962)]
142. Blinov E V et al. *Supercond. Sci. Technol.* **4** S340 (1991)
143. Dolgin A M, Smirnov S N *Sverkhprovodimost': Fiz., Khim., Tekhn.* **2** 104 (1989) [*Supercond.: Phys., Chem., Technol.* **2** 121 (1989)]
144. Khirnyi V F, Kozlovskii A A, Deyneka T G *Funct. Mater.* **8** 508 (2001)